Ruprecht-Karls University of Heidelberg

Department of Physics and Astronomy

Master thesis

A numerical study of the sign problem in the Hubbard model using a modified discrete Hubbard-Stratonovich transformation

Author:
Richard Janis Beckert
(born in Berlin, Germany)

Supervisor:
Dr. Manfred Salmhofer

A thesis submitted in fulfilment of the requirements for the degree of Master of Science in Physics

and carried out in the

Institute for Theoretical Physics

July 2013

Eidesstaatliche Erklärung

Ich versichere hiermit, dass ich diese Arbeit selbständig verfasst und außer den angegebenen keine anderen Quellen und Hilfsmittel benutzt habe.

Stockholm, den 15. Juli 2013 Richard Janis Beckert

A numerical study of the sign problem in the Hubbard model using a modified discrete Hubbard-Stratonovich transformation

The determinantal quantum Monte Carlo (DQMC) simulation of the Hubbard model relies on a discrete Hubbard-Stratonovich transformation (DHST) to decouple the Fermion interaction on every lattice site and perform importance sampling over classical variables (also called Ising fields). However, for regimes away from half-filling and inverse temperatures as low as $\beta = 4$, the method suffers from the so-called Fermion sign-problem, where the transition probabilites in the simulation are not positive definite.

Trying to improve on the sign problem, a second Ising field is introduced on every lattice point in a one-parameter family of DHSTs. The aim of this thesis is to implement the original simulation proposed in [1] and extend it to the modified DHST. We show that our implementation is accurate as it is able to recover results obtained from exact calculations. Furthermore, we show that the choice of the free parameter in the transformation has an affect on the sign.

Due to constraints in computer power the results are not conclusive.

Eine numerische Untersuchung des Vorzeichenproblems im Hubbard Modell unter der Verwendung einer erweiterten diskreten Hubbard-Stratonovich Transformation

Das Hubbard-Modell kann mit einer bestimmten Quanten-Monte-Carlo Methode numerisch gelöst werden, bei welcher die lokalen Fermion-Wechselwirkungen mit einer diskreten Hubbard-Stratonovich-Transformation (DHST) und durch Einführung von Ising-Spins auf jedem Gitterpunkt entkoppelt werden. Die resultierenden, von den Ising-Spins abhängigen Fermion-Determinanten werden dann als Übergangswahrscheinlichkeiten genutzt, um ein sogenanntes *Importance Sampling* über die Spins auszuführen. Diese in der englischsprachigen Literatur oft *DQMC* abgekürzte Methode leidet jedoch an einem Vorzeichenproblem, bei welchem Übergangswahrscheinlichkeiten für Konfigurationen weg von halber Füllung nicht immer positiv definit sind.

Der Gegenstand dieser Masterarbeit ist die Implementierung und Weiterentwicklung der ursprünglichen DQMC Methode [1]. Durch Anwendung einer erweiterten DHST wird auf jedem Gitterpunkt ein weiterer Ising-Spin eingeführt und wir erhalten einen frei wählbaren Parameter. Wir zeigen, dass unsere Implementierung akkurat ist und exakt berechnete Ergebnisse wiederspiegelt. Ebenso zeigen wir, dass die Wahl des freien Parameters einen Einfluss auf das Vorzeichenproblem hat.

Aufgrund eingeschränkter Rechenleistung können wir keine abschließende Wertung unserer Ergebnisse vornehmen.

Acknowledgements

I am grateful to Dr. Edwin Langmann, who advised and guided me on my research during my stay in Stockholm.

Contents

1. Introduction

The one-band Hubbard model is a simple model of a strongly correlated system, and is used to study magnetism in rare earth metals, phase transitions in Mott-Hubbard type insulators, and high-T_c superconductors. Despite its simple appearance, it is analytically solvable only in one dimension using the Bethe Ansatz[2].

Solutions in higher dimensions can be obtained using numerical methods such as World-Line[3], Projector[4] or Auxiliary Field Monte Carlo[1]. However, all QMC simulations of strongly coupled fermionic systems suffer from the so-called sign problem to a varying degree and already for inverse temperatures as low as $\beta = 4$ with only four lattice sites. This leads to exponential growth of the computational effort due to bad convergence. The object of this thesis is the Auxiliary Field method due to [1], which has a sign-problem away from half-filling.

In this method, the transition probabilities used in the Monte Carlo simulation are obtained by separating the electron-electron interaction and the kinetic part of the Hamiltonian using a Suzuki-Trotter decomposition. The interaction term is then replaced by an interaction of the electron with an auxiliary Ising field using a discrete Hubbard-Stratonovich transformation. The fermion degrees of freedom are subsequently traced out explicitly and written as fermionic determinants, such that the quantum partition function becomes a sum over auxiliary field configurations. The resulting expression gives the transition probabilities for the simulation, which is implemented using an algorithm originally introduced in [5].

The sign problem in the above scheme arises, because the fermionic determinants can become negative. This is a problem, as importance sampling requires a positive definite measure. Numerical studies show that the average sign decreases exponentially with the inverse temperature [6], leading to an exponential increase in the simulation time due to statistical fluctuations.

In [7] it is argued that treating the electron-electron interaction with any type of discrete Hubbard-Stratonovich transformations leads a sign problem, while in [8] it is suggested that the sign-problem is NP-hard.

Using a generalized discrete Hubbard-Stratonovich transformation, we introduce a second auxiliary field and study its effect on the sign problem in a two-dimensional lattice with 4 sites at low inverse temperatures.

2. Hubbard model

In tightly bound systems, where ion cores in the atomic lattice are separated by a distance higher than the Bohr radius of the valence band electrons, even weak interaction effects between electrons in the conduction and valence bands can drive a system towards a correlated magnetic state or an insulating phase [9]. The Hubbard model is a simple model for such a system with electrons interacting in a narrow band.

In the tight-binding approximation with localized orbitals and a strong screening of the Coulomb interaction, only a local density-density repulsion is allowed. The Hamiltonian of the one-band Hubbard model in second quantized form is given by:

$$H = H_0 + H_I = -t \sum_{\langle i,j \rangle, \sigma} \left(c^\dagger_{i,\sigma} c_{j,\sigma} + \text{h.c.} \right) + U \sum_i n_{i,\uparrow} n_{j,\downarrow}, \tag{2.1}$$

where $c^\dagger_{i,\sigma}$ and $c_{i,\sigma}$ create and annihilate fermions of spin $\sigma = \{\uparrow, \downarrow\}$ in a Wannier orbital centered at site i, respectively. The creation and annihilation operators obey the usual canonical anti-commutation relations (CAR) for fermions:

$$\left\{ c_{i,\sigma}, c^\dagger_{j,\sigma'} \right\} = \delta_{i,j} \delta_{\sigma,\sigma'} \tag{2.2a}$$

$$\left\{ c_{i,\sigma}, c_{j,\sigma'} \right\} = 0, \tag{2.2b}$$

H_0 is also referred to as the hopping term with an isotropic hopping strength t; the subscript $\langle i, j \rangle$ restricts the sum to nearest-neighbour lattice sites i and j.

In the second term, U gives the strength of the on-site Coulomb interaction, and $n_{i,\sigma} = c^\dagger_{i,\sigma} c_{i,\sigma}$ is the fermionic number operator with eigenvalues $\{0, 1\}$.

One could describe the Hubbard model phenomenologically in terms of electrons tunneling between atomic orbitals localized on individual lattice sites, with double-occupancy on a site penalized by mutual Coulomb interaction, leading to an increase in the system's energy for the repulsive $U > 0$ case.

The Hubbard model has been used to study magnetism in rare-earth metals, the Mott-Hubbard metal-insulator transition, and electronic properties of high-T_c cuprates. However, despite the simplicity of the model, no general solution to the Hubbard model exist, and the only analytic solution is for the one-dimensional model using the Bethe-ansatz. An exhaustive treatment of the solution and properties in this case is given in the monograph [10].

2.1. Some properties of the Hamiltonian

In Eq. (2.1), t and U are real numbers, which set the energy scale and fix the relative strength of the two sums contributing to the Hamiltonian. In one dimension, periodic

boundary conditions are imposed on the operators with $c_{i+L,\sigma} = c_{i,\sigma}$, with the lattice site index $i \in \{1, \dots, L\}$, and L the period of the lattice. In two dimensions we write $i \equiv (i_1, i_2)$ and $i_j \in \{1, 2, \dots, L\}$ for $j \in \{1, 2\}$, and the boundary conditions then read $c_{i+Le_j} = c_i$, where we introduce the unit vectors $e_1 = (1, 0)$ and $e_2 = (0, 1)$. Due to the boundary condition, the Hamiltonian is invariant under cyclic permutations of the lattice sites.

By acting on the vacuum state $|0\rangle$, the operators $c^\dagger_{i,\sigma}$ generate the set of states $\left|\{n_{i,\sigma}\}\right\rangle$ in the *occupation number representation*. The vacuum state is defined as the state that does not contain particles (the empty lattice), with:

$$c_{i,\sigma}|0\rangle = 0, \tag{2.3}$$

and the set of states $\left|\{n_{i,\sigma}\}\right\rangle$ span the Hilbert space $\mathcal{H}_N$ consisting of N particles:

$$\left|\{n_{i,\sigma}\}\right\rangle = \left(c^\dagger_{i_1,\sigma_1}\right)^{n_{i_1,\sigma_1}} \cdots \left(c^\dagger_{i_N,\sigma_N}\right)^{n_{i_N,\sigma_N}}|0\rangle, \tag{2.4}$$

where $n_{i,\sigma}$ is the eigenvalue of the number operator $\hat{n}_{i,\sigma} = c^\dagger_{i,\sigma}c_{i,\sigma}$ counting the number of particles on site i with spin σ. Consider acting with a number operator $\hat{n}_{j,\sigma'} = c^\dagger_{j,\sigma'}c_{j,\sigma'}$ on such a state. Then, using the commutation relation

$$[\hat{n}_{i,\sigma}, c^\dagger_{j,\sigma'}] = c^\dagger_{i,\sigma}\delta_{i,j,\sigma,\sigma'}, \tag{2.5}$$

which follows from the CAR Eq. (2.2a), we obtain:

$$\hat{n}_{j,\sigma'}\left|\{n_{i,\sigma}\}\right\rangle = = n_{j,\sigma'}\left|\{n_{i,\sigma}\}\right\rangle, \tag{2.6}$$

and therefore the possible eigenvalues of $\hat{n}_{i,\sigma}$ are $n_{i,\sigma} \in \{0, 1\}$. The fact that that there can be at most one particle in a specific fermionic state is called the *Pauli exclusion principle*.[1]

We define the Hilbert space $\mathcal{H}_2$ consisting of one lattice point (which can at most be occupied by one electron of spin $\sigma =\uparrow$ and one electron of spin $\sigma =\downarrow$) as the space spanned by the states:

$$|0\rangle = |\cdot\rangle \tag{2.7a}$$
$$c^\dagger_{i,\uparrow}|0\rangle = |\uparrow\cdot\rangle \tag{2.7b}$$
$$c^\dagger_{i,\downarrow}|0\rangle = |\cdot\downarrow\rangle \tag{2.7c}$$
$$c^\dagger_{i,\uparrow}c^\dagger_{i,\downarrow}|0\rangle = |\uparrow\downarrow\rangle, \tag{2.7d}$$

which is of dimension $\dim \mathcal{H}_2 = 4$. The Hilbert space $\mathcal{H}^{(N)}$ containing an arbitrary number N of sites is then formally constructed by the N-ary direct product:

$$\mathcal{H}^{(N)} = \underbrace{\mathcal{H}_2 \otimes \mathcal{H}_2 \otimes \cdots \otimes \mathcal{H}_2}_{N \text{ times}}, \tag{2.8}$$

[1] It can also be obtained directly from Eq. (2.2b), from which $\left(c^\dagger_{i,\sigma}\right)^2|0\rangle = 0$.

with dimension

$$\dim \mathcal{H}^{(N)} = 4^N. \tag{2.9}$$

A Hilbert space large enough to accomodate a state with an arbitrary number of particles is called a Fock state and is defined by the direct sum:

$$\mathcal{F} \equiv \bigoplus_{N=0}^{\infty} \mathcal{H}^{(N)}. \tag{2.10}$$

2.2. Symmetries of the Hubbard model

The Hubbard Hamiltonian most often found in literature is given by:

$$H = -t \sum_{\langle i,j\rangle,\sigma} \left(c_i^\dagger c_j + \text{h.c.}\right) + U \sum_i n_{\uparrow i} n_{\downarrow i} - \mu \sum_i \left(n_{\uparrow i} + n_{\downarrow i}\right), \tag{2.11}$$

where μ in the last term is the chemical potential.

The Hubbard model has symmetries, which can be made manifest by rewriting the Hamiltonian without changing its physics. To have half-filling $\langle n\rangle = 1$ occur at $\mu = 0$ (instead of at $\mu = U/2$ in the Hubard Hamiltonian), the chemical potential is rescaled[2] by $\mu \to \mu + U/2$. Then, a term $\left(\mu \sum_i 1\right)$ is added, and the Hamiltonian is further generalized by coupling the local spin to an external magnetic field, giving the final form:

$$\begin{aligned} H = &- t \sum_{\langle i,j\rangle,\sigma} \left(c_i^\dagger c_j + \text{h.c.}\right) + U \sum_i \left(n_{\uparrow i} - \frac{1}{2}\right)\left(n_{\downarrow i} - \frac{1}{2}\right) \\ &- \mu \sum_i \left(n_{\uparrow i} + n_{\downarrow i} - 1\right) - B \sum_i \left(n_{\uparrow i} - n_{\downarrow i}\right). \end{aligned} \tag{2.12}$$

This Hamiltonian is physically the same as the one we started out with, but with the additional benefit that it is now manifestly symmetric under particle-hole exchange, see below.

2.2.1. Particle-hole symmetry

The Hubbard model exhibits a couple of symmetries, e.g., under the permutation of site indices or rotation[10]. A symmetry particularly useful for Monte-Carlo simulations is the particle-hole symmetry. By knowing the results for a certain set of parameters, it immediately gives information about the corresponding symmetric set of parameters.

[2] When writing out the potential one gets an additional term $+(\sum_i U/4)$, which amounts to adding a constant to the Hamiltonian and does not change the statistics of the system. This can be seen when calculating the expectation value of some operator O:

$$\langle O\rangle = \frac{\operatorname{Tr} O \cdot \mathrm{e}^{-\beta(H+N\cdot\frac{U}{4})}}{\operatorname{Tr} \mathrm{e}^{-\beta(H+N\cdot\frac{U}{4})}} = \frac{\operatorname{Tr} O \cdot \mathrm{e}^{-\beta H}}{\operatorname{Tr} \mathrm{e}^{-\beta H}}$$

In addition, it can be used as a benchmark to check if the simulation accurately reproduces the symmetry. To show this symmetry, a so-called particle-hole transformation is performed, under which the roles of the creation and annihilation operators are interchanged:[3]

$$c_{\sigma i} \to (-1)^i c^\dagger_{\sigma i} \tag{2.13}$$
$$c^\dagger_{\sigma i} \to (-1)^i c_{\sigma i}. \tag{2.14}$$

The term $(-1)^i$ maps the Hubbard lattice onto a bipartite lattice, such that an element of the original lattice, which is now a member of the sublattice A, has neighbours which all become members of the sublattice B. Under this transformation, the hopping term of the Hubbard Hamiltonian is unchanged:

$$\begin{aligned} H_0 &= -t \sum_{\langle i,j\rangle,\sigma} \left(c^\dagger_i c_j + \text{h.c.} \right) \\ &\to -t \sum_{\langle i,j\rangle,\sigma} (-1)^{i+j} \left(c_i c^\dagger_j + \text{h.c.} \right) \\ &= -t \sum_{\langle i,j\rangle,\sigma} \left(c^\dagger_i c_j + \text{h.c.} \right), \end{aligned} \tag{2.15}$$

where the last equality is obtained using the anti-commutation relation Eq. (2.2) to exchange the operators, and noting that for a pair of next neighbours $\langle i,j\rangle$, $(-1)^{i+j} = -1$ from the definition of the bipartite lattice.

The other terms contain number operators, which transform according to:

$$n_{\sigma,i} = c^\dagger_{\sigma,i} c_{\sigma,i} \quad \longrightarrow \quad c_{\sigma,i} c^\dagger_{\sigma,i} = 1 - n_{\sigma,i}, \tag{2.16}$$

or equivalently,

$$\tilde{n}_{\sigma,i} \equiv n_{\sigma,i} - \frac{1}{2} \quad \longrightarrow -\tilde{n}_{\sigma,i}, \tag{2.17}$$

where the Hamiltonian is rewritten in terms of the last definition. We see that the interaction term stays invariant:

$$H_{\text{int}} = U \sum_i \tilde{n}_{\uparrow,i} \tilde{n}_{\downarrow,i} \qquad \longrightarrow \qquad U \sum_i \tilde{n}_{\uparrow,i} \tilde{n}_{\downarrow,i}, \tag{2.18}$$

while the chemical potential term and the coupling term to the magnetic field change:

$$H_{\text{c}} = -\mu \sum_i \left(\tilde{n}_{\uparrow,i} + \tilde{n}_{\downarrow,i} \right) \quad \longrightarrow \quad +\mu \sum_i \left(\tilde{n}_{\uparrow,i} + \tilde{n}_{\downarrow,i} \right), \tag{2.19}$$
$$H_{\text{m}} = -B \sum_i \left(\tilde{n}_{\uparrow,i} - \tilde{n}_{\downarrow,i} \right) \quad \longrightarrow \quad +B \sum_i \left(\tilde{n}_{\uparrow,i} - \tilde{n}_{\downarrow,i} \right). \tag{2.20}$$

We can thus identify a symmetry under inversion of the signs of the chemical potential and magnetic field:

$$(t, U, +\mu, +B; +\tilde{n}, +S_z) \longrightarrow (t, U, -\mu, -B; -\tilde{n}, -S_z). \tag{2.21}$$

[3]Note that in two dimensions $i = (i_1, i_2)$ and $(-1)^i \to (-1)^{i_1+i_2}$.

2.2.2. Another symmetry

Another symmetry can be seen when performing the transformation Eq. (2.14) again, but now only for down-spins, while leaving up-spins invariant:

$$c_{\uparrow,i} \longrightarrow c_{\uparrow,i} \tag{2.22a}$$
$$c^\dagger_{\uparrow,i} \longrightarrow c^\dagger_{\uparrow,i} \tag{2.22b}$$
$$c_{\downarrow,i} \longrightarrow (-1)^i c^\dagger_{\downarrow,i} \tag{2.22c}$$
$$c^\dagger_{\downarrow,i} \longrightarrow (-1)^i c_{\downarrow,i}. \tag{2.22d}$$

Under this transformation, only terms containing down-spins are changed according to Eq. (2.16):

$$H_{\text{int}} = +U \sum_i \tilde{n}_{\uparrow,i}\tilde{n}_{\downarrow,i} \quad \longrightarrow \quad -U \sum_i \tilde{n}_{\uparrow,i}\tilde{n}_{\downarrow,i} \tag{2.23}$$
$$H_{\text{c}} = -\mu \sum_i \left(\tilde{n}_{\uparrow,i} + \tilde{n}_{\downarrow,i}\right) \quad \longrightarrow \quad -\mu \sum_i \left(\tilde{n}_{\uparrow,i} - \tilde{n}_{\downarrow,i}\right) \tag{2.24}$$
$$H_{\text{m}} = -B \sum_i \left(\tilde{n}_{\uparrow,i} - \tilde{n}_{\downarrow,i}\right) \quad \longrightarrow \quad -B \sum_i \left(\tilde{n}_{\uparrow,i} + \tilde{n}_{\downarrow,i}\right). \tag{2.25}$$

Therefore, the local spin and charge operators are exchanged under the transformation Eq. (2.22d):

$$\tilde{n}_i = \tilde{n}_{\uparrow,i} + \tilde{n}_{\downarrow,i} - 1 \longleftrightarrow S_z = \tilde{n}_{\uparrow,i} - \tilde{n}_{\downarrow,i}, \tag{2.26}$$

and we thus have a direct symmetry between the repulsive $U > 0$ and attractive $U < 0$ Hubbard models under the exchange of the magnetic and chemical terms:

$$(t, U, \mu, B; \tilde{n}, S_z) \longrightarrow (t, -U, B, \mu; S_z, \tilde{n}). \tag{2.27}$$

3. Quantum Monte Carlo

The expectation value of some observable A for a system obeying the rules of quantum mechanics is calculated according to

$$\langle A \rangle = \frac{\operatorname{Tr} A \mathrm{e}^{-\beta H}}{\operatorname{Tr} \mathrm{e}^{-\beta H}}, \tag{3.1}$$

where the trace is taken over a convenient basis; the denominator is the quantum-mechanical partition function:

$$Z = \operatorname{Tr} \mathrm{e}^{-\beta H}. \tag{3.2}$$

The problem with Eq. (3.1) is the size of the Hilbert space, Eq. (2.9), for systems with even a moderate number of states: if for example we imagine a square lattice consisting of $4 \times 4 = 16$ nodes, the resulting Hilbert space will consist of 4^{16} basis states! While one could theoretically diagonalize the Hamiltonian in the basis of this small system, the number of basis states increases exponentially with the number of lattice sites, and so does the time it takes to diagonalize the Hamiltonian.

Instead of dealing with the whole Hilbert space, one can try and look at a representative sample of states, and integrate the model over a distribution of stochastically generated configurations. The generation of and averaging over randomly distributed configurations is called a Monte Carlo integration.

3.1. Monte Carlo integration

The definite integral $f(x)$ evaluated over an interval $[a, b]$ can be approximated by discretizing it using Riemann sums or applying the Simpson rule, among other methods. For example, a Riemann integral can be evaluated according to:

$$\int_a^b f(x)\,\mathrm{d}x = \Delta x \left[\frac{f(a)}{2} + \sum_{i=1}^{N-1} f(a + i\Delta x) + \frac{f(b)}{2} \right] + O(\Delta x^2), \tag{3.3}$$

where $\Delta x = {}^{(a-b)}/_{N}$, and the discretization error scales as N^{-1}. Other methods give a better convergence, but the error generally scales worse in higher dimensions — e.g., the Riemann integral scales as $N^{-1/d}$, for N points in d dimensions. The solution to this is doing a Monte Carlo integration,[1] where N random points x_i are chosen from a uniform distribution, with $a \leq x_i \leq b$. The integral can then be approximated with

$$\frac{1}{\Omega} \int_a^b f(x)\,\mathrm{d}x \cong \langle f \rangle \equiv \frac{1}{N} \sum_{i=1}^{N} f(x_i), \tag{3.4}$$

[1] See [11, 12] for a review.

where $\Omega = \int_a^b \mathrm{d}x$ is the integration volume. $\langle f \rangle$ is also called the mean of f. Since it was obtained from a set of random numbers, $\langle f \rangle$ now also has to be viewed as a random number.

The statistical error Δf in the Monte Carlo integration can be estimated using the definition of the variance as the average squared distance from the mean,

$$\mathrm{Var} f = \sigma^2 = \left\langle (f - \langle f \rangle)^2 \right\rangle, \tag{3.5}$$

and using the central limit theorem, from which we can deduce that $\langle f \rangle$ sampled from any distribution with finite variance becomes a normally distributed (Gaussian) random variable for large N. The variance in $\langle f \rangle$ is then:[2]

$$\mathrm{Var}\langle f \rangle = \frac{1}{N} \mathrm{Var} f, \tag{3.6}$$

which gives the error:

$$\Delta f = N^{-\frac{1}{2}} \sqrt{\mathrm{Var} f}. \tag{3.7}$$

While for lower dimensional problems standard integration methods yield a better convergence, in classical statistical mechanics the average of some quantity $A(p, q)$, depending on the momenta p and coordinates q, would need to be evaluated over all of phase space weighted by the statistical distribution function $\rho(p, q)$:

$$\langle A \rangle = \frac{\int A(p,q)\rho(p,q)\, \mathrm{d}p\, \mathrm{d}q}{\int \rho(p,q)\, \mathrm{d}p\, \mathrm{d}q}. \tag{3.8}$$

This amounts to an integration over $6N'$ degrees of freedom for a three dimensional system of N' particles.

3.2. Importance sampling

The error estimated by Eq. (3.6) can be reduced by reducing the effective $\mathrm{Var} f$ using a method called importance sampling. This is done by concentrating the sampling on regions where $f(x)$ is large, using a statistical weight $w(x) > 0$ with:

$$\int_a^b w(x) = 1. \tag{3.9}$$

The sampling then becomes:

$$\langle f \rangle = \int \frac{f(x)}{w(x)} w(x)\, \mathrm{d}x \cong \frac{1}{N} \sum_{i=1}^{N} \frac{f(x_i)}{w(x_i)}, \tag{3.10}$$

[2] One can view the variance of f as with respect to the uniformly distributed random numbers x_i, while the variance of $\langle f \rangle$ is actually with respect to its Gaussian distribution due to the central limit theorem.

so that the error estimate changes according to:

$$\mathrm{Var}\langle f\rangle \to \mathrm{Var}\left\langle \frac{f}{w}\right\rangle = \frac{1}{N}\,\mathrm{Var}\,\frac{f}{w}. \tag{3.11}$$

In order to keep the variance small, the distribution w should be similar to that of f. Importance sampling in the Monte Carlo method enters the simulation of a physical system naturally through the use of the partition function $Z = \sum_n \mathrm{e}^{-\beta E_n}$, where the states can be enumerated through their respective energies E_n.[3] The canonical average is then written as:

$$\langle A\rangle = \frac{\sum_n \mathrm{e}^{-\beta E_n} A}{Z}. \tag{3.12}$$

However, enumerating all states is practically impossible for systems consisting of an interesting number of sites: For example, in the relatively simple Ising model with N electrons on a grid, where each electron can have either the state up or down, we have a total of 2^N states! Instead, a subset of microstates $\{x\}_i$ with probability distribution $w(\{x\}_i)$ is generated, and the average can be written as:

$$\langle A\rangle \cong \frac{\displaystyle\sum_{i=1}^{N} \mathrm{e}^{-\beta E(\{x\}_i)} \frac{A(\{x\}_i)}{w(\{x\}_i)}}{\displaystyle\sum_{i=1}^{N} \frac{\mathrm{e}^{-\beta E(\{x\}_i)}}{w(\{x\}_i)}}, \tag{3.13}$$

where the energy and the observable now depend explicitly on one configuration $\{x\}_i$ and the average is taken with respect to all configurations $\{x\}$. Choosing the probability distribution of the microstates to be $w'(\{x\}_i) = \frac{\mathrm{e}^{-\beta E(\{x\}_i)}}{Z}$, we arrive at

$$\langle A\rangle \cong \frac{1}{N}\sum_{i=1}^{N} A(\{x\}_i). \tag{3.14}$$

3.2.1. Metropolis and heat-bath algorithms

The problem now consists in how to transform one given microstate into another. This is done using a so-called Markov process, in which the probabilities of choosing the next state $i+1$ depend entirely on the state of the immediately preceding step i.

Starting from some initial configuration $\{x\}_0$ a chain of states $\{x\}_i$ is generated via some transition probabilities $p(\{x\}_i \to \{x\}_j)$ of going from one state $\{x\}_i$ to another state $\{x\}_j$ in one step of the Markov process. To ensure that we asymptotically reach the probability w under such a Markov process, the transition probabilities are chosen such that they satisfy the *principle of detailed balance* and ergodicity. The principle of detailed balance imposes a constraint on p, that for any pair of configurations $\{x\}_i$, $\{x\}_j$ the ratio of

[3] The $\mathrm{e}^{-\beta E_n}$ are often referred to as Boltzmann weights.

probabilities to have either configuration is maintained by a direct transition between them:

$$w(\{x\}_i) \cdot p(\{x\}_i \to \{x\}_j) = w(\{x\}_j) \cdot p(\{x\}_j \to \{x\}_i). \tag{3.15}$$

Ergodicity means that it has to be possible to reach any configuration $\{x\}_j$ from any other configuration $\{x\}_i$ in a finite number of Markov steps.

The Metropolis algorithm, where the transition probability is chosen according to

$$p(\{x\}_i \to \{x\}_j) = \min\left(1, \frac{w(\{x\}_j)}{w(\{x\}_i)}\right), \tag{3.16}$$

is a simple way of ensuring that the above conditions are satisfied. To show that detailed balance is not violated, one only needs to write down the transition probabilities for the cases $w(\{x\}_i) > w(\{x\}_i)$ and the reverse $w(\{x\}_j) > w(\{x\}_i)$, as done in Table 3.1.

Table 3.1.: Transition probabilities for Metropolis algorithm

Case:	$w(i) > w(j)$	$w(j) > w(i)$
$p(i \to j)$	$\frac{w(j)}{w(i)}$	1
$w(i)p(i \to j)$	$w(j)$	$w(i)$
$p(j \to i)$	1	$\frac{w(i)}{w(j)}$
$w(j)p(j \to i)$	$w(j)$	$w(i)$

Because rows 2 and 4 are equal, the Metropolis algorithm fulfills detailed balance; adapted from [12].

An alternative choice for the transition probabilities is the so-called heat-bath algorithm:

$$p(\{x\}_i \to \{x\}_j) = \frac{w(\{x\}_j)}{w(\{x\}_i) + w(\{x\}_j)} = \frac{R}{1+R}, \tag{3.17}$$

where we have defined $R \equiv \frac{w(\{x\}_j)}{w(\{x\}_i)}$. It is easy to check that the heat-bath algorithm satisfies detailed balance. It is a good choice if the ratio $R \cong 1$ or $R \cong 0$, which would generate too many acceptances or rejections in the Metropolis algorithm.

Note that Eq. (3.7) gives the error of an average with respect to fully statistically uncorellated Markov configurations. Since in practice one generates new configurations with very small steps in between, they tend to be very similar. This leads to observables very close to each other, and in effect underestimates the statistical error.

A better estimate on the error can be generated by using techniques such as the binning or jackknife analysis, see [11] for a reference.

3.3. Auxiliary field Monte Carlo

The assumption underlying the use of a Monte Carlo integration to solve any physical system is that the probability of finding the system in some states is less likely than finding it in others: less probable states should overall contribute less to the expectation value of an operator.

Applied to the Hubbard model, the problem consists in how to transform the partition function in such a way that the terms constributing to the trace can be used as transitition probabilities when going from one configuration to the next, without explicitly diagonalizing the Hamiltonian. In fact, for strongly interacting systems and in particular fermion models on a lattice, various methods exist, all with varying degree of applicability; see [13] for a review.

In the path integral formulation of field theory, fermion operators are represented by anti-commuting c-numbers, Ψ, also called Grassmann variables. Observables bilinear in the fermion operators, i.e., of the form $O \cong \Psi^\dagger M \Psi$, with $\mathbf{M}$ an arbitrarely complex matrix, can be integrated over by performing a Gaussian integral:

$$\int \mathrm{D}\Psi^\dagger \, \mathrm{D}\Psi \mathrm{e}^{-\Psi^\dagger \mathbf{M} \Psi} = \det \mathbf{M}. \tag{3.18}$$

We therefore need to find a way to treat the Fermion-interaction, which is a term quartic in the fermion operators.

3.3.1. Hubbard-Stratonovich transformation and Suzuki-Trotter formula

The Hubbard-Stratonovich transformation provides a way to decouple a quartic interaction through an auxiliary field. The continuous form of the Hubbard-Stratonovich transformation applied to some quantum-mechanical operator O is:

$$\mathrm{e}^{\frac{1}{2}O^2} = \sqrt{2\pi} \int \mathrm{e}^{-1/2 x^2 - xO} \, \mathrm{d}x, \tag{3.19}$$

where a continuous variable x was introduced.

The kinetic and potential terms in the Hamiltonian do not commute in general, and therefore the Hubbard-Stratonovich transformation cannot be applied directly. However, one can use the so-called Suzuki-Trotter decomposition [14], which holds for two non-commuting, bounded operators A and B:

$$\mathrm{e}^{A+B} = \lim_{N \to \infty} \left(\mathrm{e}^{A/N} \mathrm{e}^{B/N} \right)^N. \tag{3.20}$$

A heuristic way of seeing this is using the Baker-Campbell-Hausdorff formula to obtain:

$$\left(\mathrm{e}^{1/N (A+B)} \right)^N = \mathrm{e}^A \mathrm{e}^B \mathrm{e}^{1/N [A,B] + O\left(N^{-2}\right)}, \tag{3.21}$$

so that the error in the breakup $\frac{1}{N}[A,B] + O\left(N^{-2}\right) \to 0$ as $N \to \infty$.

Breaking up $\beta = \Delta\tau \cdot L$ into L sizes of equal length $\Delta\tau$, the partition function is then approximated by

$$Z \cong \mathrm{Tr} \prod_{l=1}^{L} \mathrm{e}^{-\Delta\tau H_0} \mathrm{e}^{-\Delta\tau H_{\mathrm{int}}}. \tag{3.22}$$

We note that the path integral formulation of quantum mechanics provides a bridge between quantum and classical statistical mechanics: one can associate the time evolution operator, $\mathrm{e}^{-\mathrm{i}Ht}$, with the statistical Boltzmann weight by performing a Wick rotation $it \to \tau$ and identifying $\beta = \tau$. [9] In the limit $\Delta\tau \to 0$ one can therefore write (time-ordering T is important):

$$Z \cong \mathrm{Tr}\, \mathrm{T}\, \mathrm{e}^{-\int_0^\beta \mathrm{d}\tau (H_0 + H_{\mathrm{int}})}. \tag{3.23}$$

In the Hubbard model, each interaction term under the sum can be rewritten using either of the following identities, where $n = n_\uparrow + n_\downarrow$ is the local charge and $S_z = n_\uparrow - n_\downarrow$ the local spin operator:

$$n_\uparrow n_\downarrow = -1/2 S_z^2 + 1/2 n \tag{3.24a}$$
$$n_\uparrow n_\downarrow = +1/2 n^2 - 1/2 n \tag{3.24b}$$
$$n_\uparrow n_\downarrow = +1/4 n^2 - 1/4 S_z^2. \tag{3.24c}$$

Applying Eq. (3.19) and, e.g., Eq. (3.24a) at every lattice point, one obtains:

$$\mathrm{e}^{-\beta H_I} \propto \int \prod_i \mathrm{d}x_i \mathrm{e}^{-x_i^2 - \sqrt{\beta U} x_i (n_{i,\uparrow} - n_{i,\downarrow}) - \frac{\beta U}{2}(n_{i,\uparrow} + n_{i,\downarrow})}, \tag{3.25}$$

or for the partition function:

$$Z = \int \left(\prod_i \mathrm{d}x_i(\tau) \mathrm{e}^{-\int_0^\beta x_i^2(\tau)} \right) \mathrm{Tr}\, \mathrm{T}\, \mathrm{e}^{-\int_0^\beta \mathrm{d}\tau H_0 + \sum_i (U^{-1/2} x_i(\tau)(n_{i,\uparrow} - n_{i,\downarrow}) + U/2 (n_{i,\uparrow} + n_{i,\downarrow}))}, \tag{3.26}$$

where a constant prefactor has been dropped. Now that there are only bilinears appearing in the partition function, one can write it in the form

$$Z = \int \mathrm{D}x(\tau)\, \mathrm{D}\Psi^\dagger\, \mathrm{D}\Psi\, \mathrm{Tr}\, \mathrm{T}\, \mathrm{e}^{-\int_0^\beta \mathrm{d}\tau \sum_{i,j,\sigma} \Psi^\dagger_{i,\sigma} \mathbf{M}_{ij} \Psi_{j,\sigma}} \mathrm{e}^{-\sum_i \int_0^\beta x_i^2(\tau)}. \tag{3.27}$$

As shown in [5], the fermion degrees of freedom in equations of the form Eq. (3.27) can be integrated out, leaving only

$$Z = \int \mathrm{D}x(\tau) \mathrm{e}^{-\int_0^\beta x_i^2(\tau)} \det \left[\mathbb{1} + \mathrm{T}\, \mathrm{e}^{-\int_0^\beta \mathrm{d}\tau \sum_{i,j,\sigma} \Psi^\dagger_{i,\sigma} \mathbf{M}_{ij} \Psi_{j,\sigma}} \right], \tag{3.28}$$

where the argument inside the integral now has a form which can be used to calculate the transition probability between two Markov configurations.

3.3.2. Discrete Hubbard-Stratonovich transformation

Of course, $x(\tau)$ is a continuous variable, which cannot be used directly in a Monte Carlo simulation. One could try and discretize it, or alternatively try to find a discrete version of the Hubbard-Stratonovich transformations[15].

Using the same identities Eq. (3.24), auxiliary fields[4] $s = \{-1, +1\}$ are introduced at every space-time point, coupling to the local charge or spin, respectively. Equation (3.24a) is used for the repulsive $U > 0$ Hubbard model, while Eq. (3.24b) is used for the attractive $U < 0$ model. In the following, the particle-hole symmetric form of the Hubbard Hamiltonian as discussed in Section 2.2 is used.

For the repulsive case, the discrete Hubbard-Stratonovich transformation is given by:

$$\mathrm{e}^{-U\Delta\tau(n_\uparrow - 1/2)(n_\downarrow - 1/2)} = w \sum_{s=\pm 1} \mathrm{e}^{s\lambda(n_\uparrow - n_\downarrow)}, \tag{3.29}$$

with w and λ to be found. The identity can be proven by inserting all possible combinations of the eigenvalues the number operators can take, i.e., $n_\sigma = \{0, 1\}$, on both sides of Eq. (3.29). One obtains the following consistency relations, for $(n_\uparrow, n_\downarrow) = (0, 0)$ and $(1, 1)$:

$$\mathrm{e}^{-1/4 U\Delta\tau} = 2 \cdot w,$$

and for $(1, 0)$ and $(0, 1)$:

$$\begin{aligned} \mathrm{e}^{+1/4 U\Delta\tau} &= w(\mathrm{e}^{+\lambda} + \mathrm{e}^{-\lambda}) \\ &= 2w \cdot \cosh\lambda, \end{aligned}$$

which leads to the constants:

$$w = \tfrac{1}{2}\mathrm{e}^{-1/4 U\Delta\tau} \tag{3.30a}$$

$$\cosh\lambda = \mathrm{e}^{1/2 U\Delta\tau}. \tag{3.30b}$$

The final form is then:

$$\mathrm{e}^{-U\Delta\tau(n_\uparrow - 1/2)(n_\downarrow - 1/2)} = \tfrac{1}{2}\mathrm{e}^{-1/4 U\Delta\tau} \sum_{s=\pm 1} \mathrm{e}^{s\lambda(n_\uparrow - n_\downarrow)} \tag{3.31a}$$

$$= \tfrac{1}{2}\mathrm{e}^{-1/4 U\Delta\tau} \sum_{s=\pm 1} \prod_{\sigma=\uparrow,\downarrow} \mathrm{e}^{\sigma s\lambda n_\sigma}, \tag{3.31b}$$

where the contributions from the two spin channels were factorized.

The transformation of the attractive $U < 0$ Hubbard model follows the same steps, but the identity Eq. (3.24b) coupling to the local charge is used instead. Writing $U = -|U|$ and $\cosh\lambda = \mathrm{e}^{1/2|U|\Delta\tau}$ results in the decoupled form:

$$\mathrm{e}^{|U|\Delta\tau(n_\uparrow - 1/2)(n_\downarrow - 1/2)} = \tfrac{1}{2}\mathrm{e}^{-1/4|U|\Delta\tau} \sum_{s=\pm 1} \prod_{\sigma=\uparrow,\downarrow} \mathrm{e}^{s\lambda(n_\sigma - 1/2)}, \tag{3.32}$$

[4] Also referred to as Ising spins because of the similarity to the Ising model.

which is the same as Eq. (3.31), but with the spin factorizing with the same sign.

The transformation Eq. (3.31) essentially maps the d-dimensional system onto $d+1$ dimensions, where we imagine that the particles propagate between the infinitesimal imaginary time slices $\Delta\tau$. Performing it on every lattice site, the partition function Eq. (3.22) then takes the form:

$$Z = \left(\tfrac{1}{2}\mathrm{e}^{-1/4 U\Delta\tau}\right)^{L\cdot N} \operatorname*{Tr}_s \operatorname{Tr} \prod_{l=1}^{L} \mathrm{e}^{-\Delta\tau H_0} \mathrm{e}^{\sum_i s_{i,l}\lambda(n_{\uparrow,i}-n_{\downarrow,i}) + \Delta\tau\left[\mu(n_{\uparrow,i}+n_{\downarrow,i}-1)+B(n_{\uparrow,i}-n_{\downarrow,i})\right]}, \tag{3.33}$$

and factorizing the spin channels and moving the constants out,

$$= \left(\tfrac{1}{2}\mathrm{e}^{-1/4 U\Delta\tau}\mathrm{e}^{\Delta\tau\mu}\right)^{L\cdot N} \operatorname*{Tr}_s \operatorname{Tr} \prod_{l=1}^{L} \prod_{\sigma=\uparrow,\downarrow} \mathrm{e}^{-\Delta\tau H_{0,\sigma}} \mathrm{e}^{\sum_i (s_{i,l}\sigma\lambda + \Delta\tau(\mu+\sigma B)) n_{\sigma,i}}. \tag{3.34}$$

Following the convention used in [1], the terms appearing in the exponentials are now rewritten in matrix form with

$$(K)_{ij} = \begin{cases} -t & \text{for } i,j \text{ nearest neighbours,} \\ 0 & \text{otherwise,} \end{cases} \tag{3.35a}$$

$$(V^\sigma(l))_{ij} = \delta_{ij}(\lambda\sigma s_i(l) + \Delta\tau(\mu+\sigma B)), \tag{3.35b}$$

and

$$B^\sigma(l) = \mathrm{e}^{-\Delta\tau K}\mathrm{e}^{V^\sigma(l)}, \tag{3.35c}$$

where K is the $N\times N$ hopping matrix, and $(V^\sigma(l))_{ij}$ are the diagonal elements of the $N\times N$ matrix V. In one dimension, the hopping matrix has the form:

$$K_1 = -t\cdot \begin{pmatrix} 0 & 1 & 0 & \cdots & 0 & 1 \\ 1 & 0 & 1 & \cdots & 0 & 0 \\ 0 & 1 & 0 & \ddots & 0 & 0 \\ \vdots & \vdots & \ddots & \ddots & \vdots & \vdots \\ 0 & 0 & \cdots & \cdots & 0 & 1 \\ 1 & 0 & \cdots & \cdots & 1 & 0 \end{pmatrix}, \tag{3.36}$$

where the entries at matrix indices $(1,N)$ and $(N,1)$ enforce periodic boundary conditions.[5] In two dimensions, the hopping matrix permitting only nearest-neighbour hopping is constructed from

$$K_2 = \mathbb{1}_y \otimes K_{1,x} + K_{1,y} \otimes \mathbb{1}_x, \tag{3.37}$$

where $K_{1,i}$ are the one-dimensional $N_i\times N_i$ hopping matrices K_1 for dimensions $i = \{x,y\}$, respectively ($\mathbb{1}_i$ are the $N_i\times N_i$ identity matrices). We consider only lattices of up to two dimensions.

[5] Writing $\mathrm{e}^{\mathrm{i}\varphi}$ for the phase of the hopping at the boundary, the choice $\varphi = 0$ corresponds to periodic, and $\varphi = \pi$ to anti-periodic boundary conditions.

Introducing the operators

$$D_l(\sigma) \equiv \mathrm{e}^{-\Delta\tau \sum_{i,j} c_i^\dagger K_{ij} c_j} \mathrm{e}^{\sum_i c_i^\dagger V_i^\sigma(l) c_i}, \tag{3.38}$$

the partition function is rewritten in terms of the $D_l(\sigma)$:

$$Z = \operatorname*{Tr}_s \operatorname{Tr} \prod_{\sigma=\uparrow,\downarrow} \prod_{l=1}^{L} D_l(\sigma), \tag{3.39}$$

where Tr_s is the trace over the auxiliary fields $\{s\}$, and Tr is the trace over the Fermion degrees of freedom.

Finally, the trace over the fermion degrees of freedom can be taken explicitly to obtain (cf. the derivation given in Appendix A):

$$\begin{aligned} Z &= c^{L\cdot N} \operatorname*{Tr}_s \prod_\sigma \det\left[1 + B_L^\sigma B_{L-1}^\sigma \cdots B_1^\sigma\right] \\ &= c^{L\cdot N} \operatorname*{Tr}_s \det O^\uparrow \det O^\downarrow \\ &= \operatorname*{Tr}_s \rho(s). \end{aligned} \tag{3.40}$$

3.4. Observables and Green's function

Equation (3.40) has reduced the problem of performing a trace over fermionic degrees of freedom to a sum over fermionic determinants, which themselves are functions of the set of Ising spins. We can now regard the product of determinants as a Boltzmann weight in the calculation of transition probabilities and perform importance sampling over the Ising spin configurations. It turns out, that using the equal-time Green's function, the transition probability can be obtained without calculating the determinants explicitly.

The equal-time expectation value of operator A is given by:

$$\begin{aligned} \langle A \rangle &= \frac{1}{Z} \operatorname*{Tr}_s \operatorname{Tr}\left[A \prod_\sigma \prod_l D^\sigma(l)\right] \\ &= \frac{1}{Z} \operatorname*{Tr}_s \operatorname{Tr} \langle A \rangle_s \rho(s), \end{aligned} \tag{3.41}$$

where $\langle A \rangle_s$ is the average with respect to a given configuration of the Ising spins:

$$\langle A \rangle_s = \frac{\operatorname{Tr} A \prod_\sigma D^\sigma(1) \cdots D^\sigma(L)}{\rho(s)}. \tag{3.42}$$

The equal-time, single-particle Green's function with respect to a given configuration is given by (cf. Appendix B):

$$g^\sigma(l) = \left(\mathbb{1} + \mathbf{M}^\sigma(l)\right)^{-1}, \tag{3.43}$$

with

$$\mathbf{M}^{\sigma}(l) = \mathbf{B}_{l+1}\mathbf{B}_{l+2}\cdots\mathbf{B}_{L}\mathbf{B}_{1}\cdots\mathbf{B}_{l}. \tag{3.44}$$

Since particles do not interact with each other but only with the auxiliary field, Wick's theorem can be applied to Green's functions containing more particles. Note that in the following, the average is understood with respect to the Fermion trace, i.e., the average on one time slice. For example, the two-particle Green's function can be expressed in terms of one-particle Green's functions [13]:

$$\left\langle c^{\dagger}_{i_1} c_{i_2} c^{\dagger}_{i_3} c_{i_4} \right\rangle_s = \left\langle c^{\dagger}_{i_1} c_{i_2} \right\rangle_s \left\langle c^{\dagger}_{i_3} c_{i_4} \right\rangle_s + \left\langle c^{\dagger}_{i_1} c_{i_4} \right\rangle_s \left\langle c_{i_2} c^{\dagger}_{i_3} \right\rangle_s, \tag{3.45}$$

in terms of which one can express the double occupancy $\langle n_{\uparrow} n_{\downarrow} \rangle$ or spin-density correlation $\left\langle m^z_i m^z_j \right\rangle$.

The expectation of the average occupation on site i, $n_i = n_{i,\uparrow} + n_{i,\downarrow}$, can be expressed in terms of the Green's function, since $n_{\sigma,i} = c^{\dagger}_{\sigma,i} c_{\sigma,i} = 1 - c_{\sigma,i} c^{\dagger}_{\sigma,i}$:

$$\langle n_i \rangle = 2 - \left(\left\langle g^{\uparrow}_{ii} \right\rangle + \left\langle g^{\downarrow}_{ii} \right\rangle \right). \tag{3.46}$$

Similarly, the double occupation:

$$\left\langle n_{\uparrow,i} n_{\downarrow,i} \right\rangle = 1 - \left(\left\langle g^{\uparrow}_{ii} \right\rangle + \left\langle g^{\downarrow}_{ii} \right\rangle \right) + \left(\left\langle g^{\uparrow}_{ii} g^{\downarrow}_{ii} \right\rangle \right). \tag{3.47}$$

Spin-spin correlations in z-direction can be obtained through the use of $S_{zi} = n_{i,\uparrow} - n_{i,\downarrow}$ and the use of Wick's theorem Eq. (3.45):

$$\begin{aligned} \left\langle S_{zi} S_{zj} \right\rangle = \quad & \left\langle c^{\dagger}_{\uparrow,i} c_{\uparrow,i} \right\rangle \left\langle c^{\dagger}_{\uparrow,j} c_{\uparrow,j} \right\rangle + \left\langle c^{\dagger}_{\uparrow,i} c_{\uparrow,j} \right\rangle \left\langle c_{\uparrow,i} c^{\dagger}_{\uparrow,j} \right\rangle \\ & - \left\langle c^{\dagger}_{\downarrow,i} c_{\downarrow,i} \right\rangle \left\langle c^{\dagger}_{\uparrow,j} c_{\uparrow,j} \right\rangle - \left\langle c^{\dagger}_{\uparrow,i} c_{\uparrow,i} \right\rangle \left\langle c^{\dagger}_{\downarrow,j} c_{\downarrow,j} \right\rangle \\ & + \left\langle c^{\dagger}_{\downarrow,i} c_{\downarrow,i} \right\rangle \left\langle c^{\dagger}_{\downarrow,j} c_{\downarrow,j} \right\rangle + \left\langle c^{\dagger}_{\downarrow,i} c_{\downarrow,j} \right\rangle \left\langle c^{\dagger}_{\downarrow,i} c_{\downarrow,j} \right\rangle, \end{aligned} \tag{3.48}$$

which in the case $i = j$ gives the local moment.

3.5. The sign problem

In practical applications of the auxiliary field Monte Carlo method, the product of Fermion determinants and thus the probability distribution can become negative, which is a problem as the Monte Carlo method requires a positive definitve measure. Writing $\rho = \operatorname{Sgn}\rho \cdot |\rho|$, the expectation value of an observable O can then be expressed as

$$\langle O \rangle_{\rho} = \frac{\sum O\rho}{\sum \rho} = \frac{\sum O \operatorname{Sgn}(\rho) \cdot |\rho|}{\sum |\rho|} \cdot \frac{\sum |\rho|}{\sum \operatorname{Sgn}(\rho) \cdot |\rho|} = \frac{\langle O \operatorname{Sgn}(\rho) \rangle_{|\rho|}}{\langle \operatorname{Sgn}(\rho) \rangle_{|\rho|}}, \tag{3.49}$$

where importance sampling is now performed with respect to the absolute value of the probability distribution, $|\rho|$, and where the final result has to be divided by the average value of the sign. With that definition, the average value of the sign sampled with respect to the absolute probability density is the ratio:

$$\langle \operatorname{Sgn} \rangle = \frac{\tilde{Z}}{Z}, \tag{3.50}$$

where $\tilde{Z}$ the partition function with respect to $|\rho|$ and Z with respect to ρ.

When the average sign is close to unity, $|\rho|$ should be a good guiding function for the random walk. If it is far away from unity however, it is likely that the sampling is predominantly done in unimportant regions of phase space. Furthermore, large fluctuations in the sign and therefore in the measured observables lead to large cancellations in both $\langle O\,\mathrm{Sgn}\rangle$ and $\langle \mathrm{Sgn}\rangle$ and therefore in the variance of the simulation.

Using Eq. (3.6) and given a set of N random configurations $\{x_1, \ldots, x_N\}$, we can estimate the error for very small $\langle \mathrm{Sgn}\rangle = \varepsilon \ll 1$ as:

$$\mathrm{Var}\langle \mathrm{Sgn}\rangle = \frac{1}{N}\,\mathrm{Var}\,\mathrm{Sgn} = \frac{1}{N}\left\langle \mathrm{Sgn}^2\right\rangle - \langle \mathrm{Sgn}\rangle^2 \cong \frac{1}{N}, \tag{3.51}$$

from which the relative error is

$$\triangle_r = \frac{1}{\sqrt{N}\varepsilon}. \tag{3.52}$$

For example [13], assuming an average sign of $\langle \mathrm{Sgn}\rangle = 0.5$, if one tries to achieve relative accuracy of just 1%, a number of 40,000 stochastically independent samples is needed.

Using the Ground-State algorithm [6][6] and the auxiliary field method [16] with $t = 0$, it was shown numerically that the average sign declines exponentially with inverse temperature, where the constant c is depending on the system size and potential coupling U:

$$\langle \mathrm{Sgn}\rangle \propto \mathrm{e}^{-\beta c}. \tag{3.53}$$

Furthermore, the slope of this decay is not unique and must depend on the particular path integral formulation used. In particular, the transformation scheme used to decouple the electron-electron interaction in the auxiliary field method has an influence on the average sign. This further suggests that the sign problem is not an intrinsic property of the model Hamiltonian, but an artifact of the decoupling scheme, which any method using a discrete Hubbard-Stratonovich transformation suffers from [7, 16].

The attractive Hubbard model does not suffer from the sign problem (at least in the absence of a magnetic field, $B = 0$), and neither does the repulsive Hubbard model at half filling. Both cases are discussed in Appendix D.

3.6. Generalized discrete Hubbard-Stratonovich transformation

In [15] it was suggested[7] to use a modified transformation with second auxiliary field and a complex prefactor coupling to the local charge. However, the resulting consistency relations were chosen such that they do not allow for a free parameter.

[6] In [6] a few data points from a Grand Canonical auxiliary field simulation are shown, but these have either extremely large error bars or do not agree with the least-squares fit. The same has to be said for the results obtained by [16] for $t = 0$.

[7] Cf. the erratum [17].

Following [18] we therefore use an alternative decoupling scheme and introduce a second spin auxiliary field coupling to the local charge of the form:

$$\mathrm{e}^{-\Delta\tau U(n_\uparrow - 1/2)(n_\downarrow - 1/2)} = w \sum_{s_1, s_2 = \pm 1} \mathrm{e}^{\lambda_1 s_1 (n_\uparrow - n_\downarrow) + \lambda_2 s_2 (n_\uparrow + n_\downarrow - 1)}, \tag{3.54}$$

which leads to the consistency relations:

$$\mathrm{e}^{\frac{-\Delta\tau U}{4}} = 4w \cosh(\lambda_2) \tag{3.55a}$$

$$\mathrm{e}^{\frac{\Delta\tau U}{4}} = 4w \cosh(\lambda_1), \tag{3.55b}$$

and finally

$$\cosh(\lambda_1) = \cosh(\lambda_2) \mathrm{e}^{\frac{\Delta\tau U}{2}}. \tag{3.56}$$

The result Eq. (3.54) is a one-parameter family of transformations depending on λ_2. In the limit $\lambda_2 \to 0$, the standard transformation Eq. (3.31) is recovered, while the limit $\lambda_1 \to 0$ recovers the transformation for the attractive case, Eq. (3.32).

The partition function with the decoupled electron-electron interaction then reads (dropping the constant term in front of the partition function):

$$Z = \operatorname*{Tr}_s \mathrm{e}^{\lambda_2 \sum_{i,l} s_{2,i,l}} \operatorname{Tr} \prod_{l=1}^{L} \prod_{\sigma = \uparrow, \downarrow} \mathrm{e}^{-\Delta\tau H_{0,\sigma}} \mathrm{e}^{\sum_i (\sigma \lambda_1 s_{1,i,l} + \lambda_2 s_{2,i,l} + \Delta\tau(\mu + \sigma B)) n_{\sigma,i}}, \tag{3.57}$$

and the matrix of the transformed potential term Eq. (3.35b) becomes:

$$\left(V^\sigma(l)\right)_{ij} = \delta_{ij} \left[\lambda_1 \sigma s_{1,i}(l) + \lambda_2 s_{2,i}(l) + \Delta\tau(\mu + \sigma B)\right]. \tag{3.58}$$

With these changes one can investigate how the average sign depends on the choice of the free parameter λ_2, and in particular how the constant c in Eq. (3.53) is affected.

We further note that one can choose the transformation Eq. (3.54) with a different λ_2 on every space-time point, giving a total of $N \cdot L$ free parameters.

4. Algorithm

When performing a full Monte Carlo simulation over a space-time lattice of the Hubbard model, one generates successive Markov configurations by going over all space-points and trying to flip each spin, one time-slice at a time. Each spin is flipped according to a transition probability, cf. Section 3.2.1.

4.1. Transition probability

Calculating the transition probability via the determinants of Eq. (3.40) is not feasible in practice, especially when one considers larger systems (with bigger matrices). In [5] an algorithm was introduced, by which the transition probability can be expressed in terms of Green's functions, Eq. (3.43). The ratio between the determinant products of two spin configurations s and s' is:

$$R = \frac{\rho(s')}{\rho(s)} = \frac{\det O^{\uparrow}(s')}{\det O^{\uparrow}(s)} \cdot \frac{\det O^{\downarrow}(s')}{\det O^{\downarrow}(s)} \equiv R^{\uparrow} R^{\downarrow}. \tag{4.1}$$

The most simple transitition between two Markov configurations involves flipping at most one spin at a time, and s and s' are those configurations which differ only by one spin. By flip we mean the change of the matrix element ii on the timeslice l in Eq. (3.35b) due the inversion $s_i(l) \to -s_i(l)$:

$$\Delta(V^{\sigma}(l))_{ij} \equiv \left[V^{\sigma}(l, -s_i(l))\right]_{ij} - \left[V^{\sigma}(l, s_i(l))\right]_{ij} = -\delta_{ij} 2\sigma\lambda s_i(l). \tag{4.2}$$

Accordingly, the matrices $\mathbf{B}^{\sigma}(l)$, Eq. (3.35c), are also changed:

$$\mathbf{B}^{\sigma}(l) \to \mathbf{B}^{\sigma}(l)\ \triangle_i^{\sigma}\ (l), \tag{4.3}$$

$$\left(\triangle_i^{\sigma}(l)\right)_{jk} = \begin{cases} 0 & , j \neq k \\ 1 & , j = k \neq i \\ \mathrm{e}^{-2\sigma\lambda s_i(l)} & , j = k = i \end{cases}. \tag{4.4}$$

The ratio R^{σ} can then be written in the simple form, cf. Appendix C:

$$R^{\sigma} = 1 + \left(1 - \left(g^{\sigma}(l)\right)_{ii}\right)\left(\mathrm{e}^{-2\sigma\lambda s_i(l)} - 1\right), \tag{4.5}$$

and is used in the calculation of the transition probabilities in the heat-bath algorithm:

$$P = \frac{R^{\uparrow} R^{\downarrow}}{1 + R^{\uparrow} R^{\downarrow}}. \tag{4.6}$$

4.2. Updating the Green's function

Through the change of the i-th element in the matrix $\mathbf{B}(l)$, the Green's function $g^\sigma(l)$ is also affected and needs to be updated. Following along similar lines that lead to Eq. (4.5), one can relate the new Green's function to the old one:

$$g'^\sigma(l) = \left(g^\sigma(l) + (\mathbb{1} - g^\sigma(l))\ \triangle_i^\sigma\ (l)\right)^{-1} g^\sigma(l) \tag{4.7a}$$

$$= g^\sigma(l) - \left((\mathbb{1} - g^\sigma)(\triangle_i^\sigma(l) - \mathbb{1})\right) g'^\sigma(l) \tag{4.7b}$$

which is a Dyson-type equation[13], and the solution of which leads to the explicit form for a matrix element jk of the new Green's function:

$$\left(g'^\sigma(l)\right)_{jk} = g^\sigma(l) + \frac{g_{ik}^\sigma(l)\left[g_{ji}^\sigma(l) - \delta_{ij}\right]}{\left(\mathrm{e}^{-2\sigma\lambda s_i(l)} - 1\right)^{-1} + \left(1 - g_{ii}^\sigma(l)\right)}. \tag{4.7c}$$

4.3. Propagation of the Green's function

After an attempted flip of each space-point of one time-slice, the Green's function needs to be propagated to the next time slices, $g^\sigma(l+1)$. Instead of recalculating the full matrix, one can instead wrap the old one:

$$g^\sigma(l+1) = \mathbf{B}_l^\sigma \cdot g^\sigma(l) \cdot \left(\mathbf{B}^\sigma(l)\right)^{-1}. \tag{4.8}$$

In practice one has to be careful about this wrapping of the Green's function, as it causes the new Green's function to deteriorate after many iterations. After m propagations through Eq. (4.8) have been performed, a new Green's function needs to be recalculated from scratch, and then compared to the wrapped result. This can suggest whether to de- or increase m.

4.4. Matrix stabilization

For inverse temperatures $\beta \geq \frac{4}{t}$, the Green's function Eq. (3.43) cannot be calculated directly by straight-forward matrix multiplication and subsequent inversion: the matrices involved in the calculation become ill-conditioned and numerical instabilities are encountered.

For the case $U = 0$, the eigenvalues of $\mathbf{M}^\sigma(l)$ range from $\mathrm{e}^{+t\beta}$ to $\mathrm{e}^{-t\beta}$, which get buried by the larger contributions for large β because all operations are performed on a machine of finite precision. This also leads to the problem that for some configurations of the Ising spins a numerical instability is encountered during the inversion leading to Eq. (3.43).

Following [19], this problem can be treated by decomposing the ill-conditioned matrix into the form **UDV** using the Modified Gram-Schmidt (MGS) factorization,[1] where **U** is

[1] The usual method for performing multiplications of ill-conditioned matrices is the very stable singular-value decomposition (SVD), where **U** and **V** are additionally chosen to be orthogonal. However, compared to MGS it adds to computational complexity.

orthogonal, **V** unit triangular, and **D** diagonal; the latter contains the diverging singular values.[2]

The process is then as follows: assume we can stably generate the product of m of the $\mathbf{B}^\sigma(l)$ matrices entering $\mathbf{M}^\sigma(l)$ starting from the right. This product is then factorized using the above scheme to obtain:

$$\begin{aligned}\mathbf{m}_1^\sigma(l) &= \mathbf{B}_{l-m+1}^\sigma \cdots \mathbf{B}_{l-1}^\sigma \cdot \mathbf{B}_l^\sigma \\ &= \mathbf{U}_1^\sigma \mathbf{D}_1^\sigma \mathbf{V}_1^\sigma,\end{aligned} \tag{4.9}$$

using which the next m multiplications moving to the left are obtained:

$$\begin{aligned}\mathbf{m}_2^\sigma(l) &= \mathbf{B}_{l-2m+1}^\sigma \cdots \mathbf{B}_{l-2m+1}^\sigma \cdot \mathbf{U}_1^\sigma \mathbf{D}_1^\sigma \mathbf{V}_1^\sigma \\ &= \mathbf{U}_2^\sigma \mathbf{D}_2^\sigma \mathbf{V}'^\sigma \mathbf{V}_1^\sigma \\ &= \mathbf{U}_2^\sigma \mathbf{D}_2^\sigma \mathbf{V}_2^\sigma.\end{aligned} \tag{4.10}$$

The process is repeated L/m times to obtain the decomposed version of $M^\sigma(l)$. Then, when adding the unit matrix, the different matrices are kept separate:

$$g^{\sigma-1}(l) = \mathbb{1} + \mathbf{M}^\sigma(l) \tag{4.11a}$$

$$= \mathbf{U}_{L/m}^\sigma \left(\mathbf{U}_{L/m}^{\sigma-1}\mathbf{V}_{L/m}^{\sigma-1} + \mathbf{D}_{L/m}^\sigma\right)\mathbf{V}_{L/m}^\sigma. \tag{4.11b}$$

Finally, the middle factor is again decomposed:

$$= \mathbf{U}_{L/m}^\sigma \mathbf{U}'^\sigma \mathbf{D}^\sigma \mathbf{V}'^\sigma \mathbf{V}_{L/m}^\sigma \tag{4.11c}$$

to obtain the result

$$g^\sigma(l) = \mathbf{V}^{\sigma-1}\mathbf{D}^{\sigma-1}\mathbf{U}^{\sigma-1}. \tag{4.11d}$$

4.5. Storing partial products

Since the propagation of the wrapping involves a block of m matrices $\mathbf{B}_l^\sigma$, at most m of these matrices will change their position, and the order of the remaining ones will stay constant. If we multiply from the right, we observe that a change in an earlier calculated factor $(\mathbf{UDV})_{i-1}$ affects later factors $(\mathbf{UDV})_i$. However, if we start multiplying the matrices $\mathbf{B}_l^\sigma$ from the left and factorize in reverse order, earlier factors $i-1$ are not affected if a change occurs in a right-standing matrix. Doing this, we obtain a total of L/m factors $(\mathbf{VDU})_j$. Then, when moving one block of matrices to the other side of $\mathbf{M}^\sigma(l)$ to calculate $\mathbf{M}^\sigma(l+m)$, the previous block $(\mathbf{VDU})_{j-1}$ can be recalled from memory. For example, at $l=0$ we get:

$$\mathbf{M}^\sigma(0) = \underbrace{\underbrace{\underbrace{\mathbf{B}_1^\sigma \cdots \mathbf{B}_m^\sigma}_{(\mathbf{VDU})_1} \cdots \mathbf{B}_{L-2m+1}^\sigma}_{(\mathbf{VDU})_{L/m-1}} \cdots \mathbf{B}_{L-m}^\sigma}_{(\mathbf{VDU})_{L/m}} \cdots \mathbf{B}_{L-m+1}^\sigma \cdots \mathbf{B}_L^\sigma, \tag{4.12}$$

[2] This method is usually called **QR**-decomposition, with **Q** orthogonal and **R** upper triangular; **R** can be further decomposed into $\mathbf{R} = \mathbf{DV}$.

and at $l = m$ we need to calculate the first block of the **UDV** decomposition

$$\mathbf{M}^{\sigma}(m) = \underbrace{\mathbf{B}^{\sigma}_{L-m+1} \cdots \mathbf{B}^{\sigma}_{L}}_{(\mathbf{UDV})_1} \cdot (\mathbf{VDU})_{L/m-1}\,, \tag{4.13}$$

so that at $l = 2m$ $(\mathbf{UDV})_1$ can be used to calculate the next

$$\mathbf{M}^{\sigma}(2m) = \underbrace{\mathbf{B}^{\sigma}_{L-2m+1} \cdots \mathbf{B}^{\sigma}_{L-2m} (\mathbf{UDV})_1}_{(\mathbf{UDV})_2} \cdot (\mathbf{VDU})_{L/m-1}\,. \tag{4.14}$$

For general $\mathbf{M}^{\sigma}(t)$, writing $t = k \cdot m$, $k \in \{0, 1 \ldots, L/m\}$, we get:

$$\mathbf{M}^{\sigma}(t) = (\mathbf{UDV})_t \cdot (\mathbf{VDU})_{L/m-t}\,. \tag{4.15}$$

Sweeping back and forth through the space-time lattice, the partial products $(\mathrm{UDV})_i$ and $(\mathrm{VDU})_j$ can now be used where needed, and only the changed products of $\mathbf{B}^{\sigma}_l$ need to be recalculated from scratch.

The expression for the calculation of the Green's function, again making sure to keep the different matrices separate, changes to:

$$\begin{aligned} g^{\sigma-1}(t) &= \mathbf{U}^{\sigma}_t \left(\mathbf{U}^{\sigma-1}_t \mathbf{U}^{\sigma-1}_{L/m-t} + \mathbf{D}^{\sigma}_t \mathbf{V}^{\sigma}_t \mathbf{V}^{\sigma}_{L/m-t} \mathbf{D}^{\sigma}_{L/m-t}\right) \mathbf{U}^{\sigma}_{L/m-t} \\ &= \mathbf{U}^{\sigma}_t \mathbf{U}'^{\sigma} \mathbf{D}'^{\sigma} \mathbf{V}'^{\sigma} \mathbf{U}^{\sigma}_{L/m-t} \qquad (4.16a) \\ g^{\sigma}(t) &= \mathbf{U}^{\sigma-1}_{L/m-t} \mathbf{V}'^{\sigma-1} \mathbf{D}'^{\sigma-1} \mathbf{U}'^{\sigma-1} \mathbf{U}^{\sigma-1}_t. \qquad (4.16b) \end{aligned}$$

4.6. Taking measurements

Given one configuration of auxiliary fields, the equal-time Green's functions for different time-slices are calculated according to Appendix B, and using the same propagation and stabilization procedures as described in above.

The ensemble average of the particle occupation is the average over all space-time points, and can be obtained directly from the Green's function (cf. Eq. (3.46)):

$$\langle n \rangle = 2 - \frac{1}{LN_s} \sum_{i,l} \sum_{\sigma} \left\langle \left(g^{\sigma}(l)\right)_{ii} \right\rangle. \tag{4.17}$$

The Green's function itself is averaged over all n_{mc} configurations of Ising spins obtained through importance sampling:

$$\left\langle \left(g^{\sigma}(l)\right)_{ij} \right\rangle = \frac{1}{n_{\mathrm{mc}}} \sum_{k=1}^{n_{\mathrm{mc}}} \left(g^{\sigma}_k(l)\right)_{ij}, \tag{4.18}$$

where k denotes the k-th spin configuration. Double occupancy and spin-spin correlation are obtained along the same lines.

4.7. Computational complexity

To justify the above manipulations, one needs to discuss the time complexity of the various calculations performed during one Monte Carlo sweep over the entire space-time lattice.

Consider a lattice of N nodes in each spatial direction d, which corresponds to the square $\mathbf{B}_l^\sigma$ matrix of dimensions $N_s \times N_s$, where $N_s = N^d$ the total number of nodes. With a total of L time slices, multiplying all $\mathbf{B}_l^\sigma$ requires $\sim (L-1) \cdot N^{3d}$ steps. The final calculation of the actual Fermion determinant takes $\sim N^{3d}$ steps. Clearly, recalculating the Fermion determinant every time the underlying Ising spin matrix changes is clearly not feasible, as it would amount to up to $\sim L^2 N^{4d}$ steps when sweeping through the entire lattice.

Through the application of the techniques discussed above, one can reduce the time complexity to $\sim \frac{L}{m}\frac{L}{m'}LN^{3d}$ and finally $\sim \frac{L}{m}LN^{3d}$ when storing partial products in memory. Recalling that the number of time slices is related to the inverse temperature through $\beta = \frac{L}{\Delta\tau}$, the amount of calculations is greatly reduced especially for low temperatures and large system sizes. Finally, this procedure also grants direct access to the Green's function for measurement and calculation of other observables.

The time complexity of the various procedures in the Monte Carlo simulation is summarized in Table 4.1.

Table 4.1.: Time complexity for procedures in the Monte Carlo simulation (big-O notation)

Process	Number of steps
Elementary operations	
Vector-vector multiplication	$O(N^{2d})$
Matrix-matrix multiplication	$O(N^{3d})$
Inversion	$O(N^{3d})$
Factorization	$O(N^{3d})$
From scratch	
Determinant	$O(L \cdot N^{3d})$
Green's	$O(L \cdot N^{3d})$
Using properties of Green's function	
Green's update	$O(N^{2d})$
Wrapping	$O(N^{3d})$
Full sweep	
Naive	$O(L^2 N^{4d})$
With stabilization	$O\left(\frac{L}{m}\frac{L}{m'} \cdot LN^{3d}\right)$
With Partial products	$O\left(\frac{L}{m} \cdot LN^{3d}\right)$

N denotes the number of lattice sites in d spatial dimensions, L the number of time slices, m the number of steps after which the Green's function is recalculated from scatch, m' the number matrices in each factorization group.

5. The program

5.1. Choice of tools

The algorithm discussed in Chapter 4 was implemented in `Python 3.3` using the `NumPy 1.7` and `SciPy 0.12` libraries[20] for linear algebra routines, and `h5py 2.1` to store simulation results in the `HDF5` format[21]. The programming language was chosen because it allows for fast prototyping, while the mentioned libraries provide wrapper functions to the optimized `BLAS` and `LAPACK` linear algebra libraries (in this case through the `Intel Math Kernel Library 11.0`[22]). It also allows for future optimization by rewriting expensive operations such as the update of the Green's functions in the `C` language, which can then be exposed to the rest of the program using the `Cython` compiler. The `HDF5` file format allows to easily write and read the large matrices generated in the simulation (e.g., measured Green's functions or lattices representing spin configurations).

While `Fortran 90/95` or `C` are frequently used languages when performing numerical simulations as they allow for programming close to the hardware, their low-level nature requires a lot of care and time when implementing a complex algorithm. Furthermore, because the bulk of the work of the algorithms is performed within the `BLAS` and `LAPACK` libraries, which are themselves implemented in fine-tuned `Fortran`, the speed-gain should be limited (this, however, needs investigation).

At of the time of this writing, we only found the `QUEST`[23] software as a reference implementation of a DQMC simulation, which was used in [24]. However, the program's source is very extensive (amounting to several 10,000 lines of `Fortran` code), and not well documented. We therefore chose not to try and extend it and rely on our own implementation instead.

5.2. Implementation

The rough outline of the program is as follows:

1. Obtain system parameters (e.g., inverse temperature β, slice-length $\Delta\tau$, system size N, number n_{mc} of Monte Carlo interations) from a configuration file.
2. Construct the lattice from a set of uniformly distributed random numbers $\{-1, +1\}$ for each of the N lattice sites on all $L = \frac{\beta}{\Delta\tau}$ time slices, and calculate all necessary quantities.
3. Generate new spin-configurations by sweeping through the space-time lattice, trying to flip each spin s on each slice with probability Eq. (4.6), one at a time.
   - Repeat n_{mc} number of times.

A naive implementation of the sweep through the space-time lattice without matrix stabilization and other optimizations is shown in Algorithm 1 using pseudo-code. Note that when introducing a second Ising spin s' on each space-time point as in Section 3.6, one first tries to flip $s_{i,l}$ followed by $s'_{i,l}$ with their respective probabilities. Configurations and Green's functions are updated after each flip, if necessary.

Algorithm 1 Naive sweep through the space-time lattice

Require: $\mathbf{K}, \lambda, N, L$

procedure SWEEP($\{s_{1,1}, \dots, s_{N,1}, \dots, s_{1,L}, \dots, s_{N,L}\}, \mathbf{g}^\sigma(1)$)
  for $l \leftarrow 1, L$ **do**
    for $i \leftarrow 1, N$ **do**
      $s \leftarrow s_{i,l}$
      $g \leftarrow [\mathbf{g}^\sigma(l)]_{i,i}$
      $R^\sigma \leftarrow 1 + (1-g)\left(\mathrm{e}^{-2\sigma\lambda s} - 1\right)$ ▷ σ meant as $\sigma = \{\uparrow, \downarrow\}$
      $Y \leftarrow \mathrm{ABS}(\frac{R^\uparrow R^\downarrow}{1+R^\uparrow R^\downarrow})$ ▷ Heat-bath algorithm
      if RAND$(0,1) < Y$ **then**
        $s_{i,l} \leftarrow -s_{i,l}$
        $\mathbf{g}^\sigma(l) \leftarrow$ UPDATE$(g^\sigma(l), i, s)$
      end if
    end for
    $\mathbf{B}^\sigma(l) \leftarrow \mathrm{e}^{\mathbf{K}}\mathrm{e}^{\sigma\lambda\{s_{1,l},\dots,s_{N,l}\}}$
    $\mathbf{g}^\sigma(l+1) \leftarrow \mathbf{B}^\sigma(l)\mathbf{g}^\sigma(l)\mathbf{B}^{\sigma-1}(l)$ ▷ Wrapping
  end for
end procedure

procedure UPDATE$(g^\sigma(l), i, s)$
  for $j, k \leftarrow 1, N$ **do**
    $[g^\sigma(l)]_{j,k} \leftarrow [g^\sigma(l)]_{j,k} + \frac{[g^\sigma(l)]_{ik}\left([g^\sigma(l)]_{ji} - \delta_{ij}\right)}{\left(\mathrm{e}^{-2\sigma\lambda s}-1\right)^{-1} + (1-g)}$
  end for
end procedure

In principle, a set of Green's functions $g^\sigma(l)$ can be measured[1] after each attempt of flipping a spin, but since their calculation is computationally expensive, cf. Section 4.7, the measurements should be performed once a sufficiently statistically uncorrelated Markov configuration was obtained. We follow [1, 13] and take measurements after one complete sweep of the space-time lattice is performed.

[1] By a measurement we mean the calculation of a set of Green's functions for the different times l using one configuration of the underlying spin-lattice.

5.3. Frequency of stabilization

In Sections 4.4 and 4.5 we introduced the parameters m and m' for the frequency of recalculating the Green's functions and the number of stable multiplications of the matrices $\mathbf{B}^{\sigma}(l)$, respectively. Following [25], we chose to set $m = m'$ and require $t \cdot \Delta\tau \cdot m \leq 1.5$. This resulted in the Green's functions deviating by less than 0.1% in every element due to propagation through wrapping.

For simulations involving a second Ising spin, requiring $t \cdot \Delta\tau \cdot m \leq 1.3$ was sufficient to ensure that the matrix multiplications were not resulting in numerical singularities when performing the inversions which enter the Green's function.

6. Results

6.1. Optimal size of Trotter breakup $\Delta\tau$

In order to check the validity of the program, we performed a number of tests for a small system consisting of two sites in one dimension. Measurements were taken every time two sweeps through the entire space-time lattice were completed.

First, it had to be determined how small $\Delta\tau$ has to be chosen in order to get a small systematic error due to the Trotter breakup, while keeping the number L of time slices to a minimum as to not unnecessarily increase computational complexity. Table 6.1 shows results for the double occupancy, $\langle n_\uparrow n_\downarrow \rangle$, at an inverse temperature of $\beta = 2$. We compare with numerical and exact results quoted in [15] and find that a breakup of $\Delta\tau = 0.125$ is adequate.

The break-up size $\Delta\tau = 0.125$ is mentioned as a good trade-off between accuracy and computational complexity in the literature [15], and a value of $\Delta\tau = \frac{1}{8 \cdot t}$ is suggested [25]. Halving $\Delta\tau$ roughly doubles the run-time of the same number of sweeps.

Table 6.1.: Double occupancy $\langle n_\uparrow n_\downarrow \rangle$ for different break-up sizes

$(\Delta\tau)^{-1}$	Our results	Hirsch's results [15]
2	0.0587(8)	0.0580(5)
4	0.1103(9)	0.1100(5)
8	0.1317(9)	0.1310(3)
16	0.1382(9)	0.1363(5)
32	0.1376(9)	—
exact	0.1384	—

Parameters: $\beta = 2$, $t = 1$, $U = 4$, $\mu = 0$, $B = 0$, $N = 2$, $n_{\text{mc}} = 2048$; exact result taken from [15].

Runtimes for $n_{\text{mc}} = 2048$ sweeps through space-time lattices at $\beta = 6$ with $\Delta\tau = 0.125$ and different numbers N of sites are shown in Table 6.2. The simulations were performed on a laptop using an Intel `i5-520m` processor running one thread.

6.2. Particle-hole symmetry

An important test is whether the program is able to reproduce the symmetries in Section 2.2. In particular, it needed to be tested whether a simulation with two Ising spins

Table 6.2.: Runtimes in minutes for 2048 sweeps through the space-time lattice with $l = 96$ slices

System	1 Ising spin	2 Ising spins
1D, 2 sites	1:50	2:15
1D, 4 sites	2:30	2:50
2D, 64 sites	19:30	31:20

Doubling the number of sites does not directly double the runtime. We believe that for small system sizes the overhead from using wrapped `LAPACK` routines is still significant; the program spends as much time looking up routines as it does calculating matrices.

from the transformation Eq. (3.54) recovers the same results.

Using $\beta = 6$, $t = 1$, $U = \pm 4$, $\Delta\tau = 0.125$ and setting $B = 0$ for the simulation of the repulsive model (and equivalently $\mu = 0$ for the attractive one), the program shows both symmetries with $n_{\mathrm{mc}} = 2048$ sweeps, see Fig. 6.1. We observe that the particle hole symmetry $(t, U, +\mu, +B; +\tilde{n}, +S_z) \rightarrow (t, U, -\mu, -B; -\tilde{n}, -S_z)$, Eq. (2.21), is recovered by the simulation, as the plot is point symmetric about half-filling. Also, the symmetry between the repulsive and attractive models, $(t, +U, \mu, B; \tilde{n}, S_z) \rightarrow (t, -U, B, \mu; S_z, \tilde{n})$, Eq. (2.27), is recovered, since the results of $\langle \tilde{n} \rangle$ for $U > 0$ and $\langle S_z \rangle$ for $U < 0$ map onto each other.

The data points obtained with parameters $\lambda_2 = 0.1$ and $\lambda_2 = 0.5$ in a simulation of two Ising spins give results very similar to the $\lambda_2 = 0.0$ case and are therefore not plotted (the plots look identical). The error bars lie inside the datapoints and the agreement with the exact solution, which was obtained from a diagonalization of the Hamiltonian [26], is very good.

Some numerical results for the region $\mu = \pm 0.6 \cdot U$, which appears to have the least accuracy, are given in Table 6.3 (for $U < 0$ and $\langle S_z \rangle$ the data is similar). The relative error is about 3% and all measurements agree with each other within their error bars. We assume that the difference to the exact solution is due to Trotter breakup.

6.3. The sign problem

For systems consisting of $N = 2$ sites, we did not measure a negative sign even for inverse temperatures as high as $\beta = 10$. Increasing the number of sites to $N = 4$, we observed negative signs already for inverse temperatures as low as $\beta = 2$, which however were so infrequent that $\langle \mathrm{Sgn} \rangle \simeq 1$ for all practical purposes. Results for larger values of β are given in Fig. 6.2. We have to note that we are not able to give reliable estimates of the statistical error for our results because of constraints in computational power, cf. the discussion in Chapter 7.

We observe that there is no sign problem at half-filling and for $\mu \rightarrow U$. The average

Table 6.3.: Some results for $\langle n \rangle$

μ	λ_2	$\langle n \rangle$	Δ
+2.4	0.0	0.2637	$\pm$0.0068
	0.1	0.2587	$\pm$0.0091
	0.5	0.2700	$\pm$0.0076
−2.4	0.0	−0.2718	$\pm$0.0069
	0.1	−0.2731	$\pm$0.0052
	0.5	−0.2849	$\pm$0.0074
Exact result	0.2824	——	

Parameters: $\beta = 6$, $t = 1$, $U = 4$, $B = 0.0$, $N = 2$, $n_{\text{mc}} = 2048$

Figure 6.1.: Symmetries of the Hubbard model

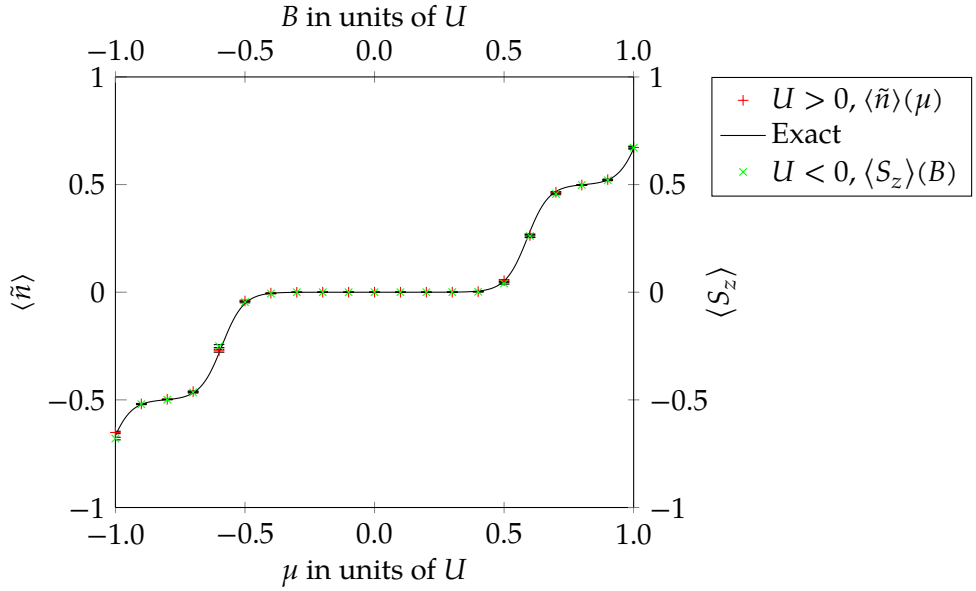

Parameters: $\beta = 6$, $t = 1$, $U = 4$, $N = 2$, $n_{\text{mc}} = 2048$

sign seems to be symmetric with respect to half-filling, and becomes bad in the interval $\mu = \pm[0.2, 0.6]$, which roughly corresponds to a region of quarter- and three-quarter-filling. The data obtained in Fig. 6.2 was generated with 2^{16} measurements of Sgn corresponding to the same number n_{mc} of sweeps through the lattice. The simulation of one set of parameters took up to 01:30h for $\beta = 8$.

For reference, the lowest average values for each β are given in Table 6.4.

Figure 6.2.: $\langle \text{Sgn} \rangle$ as a function of μ at different β

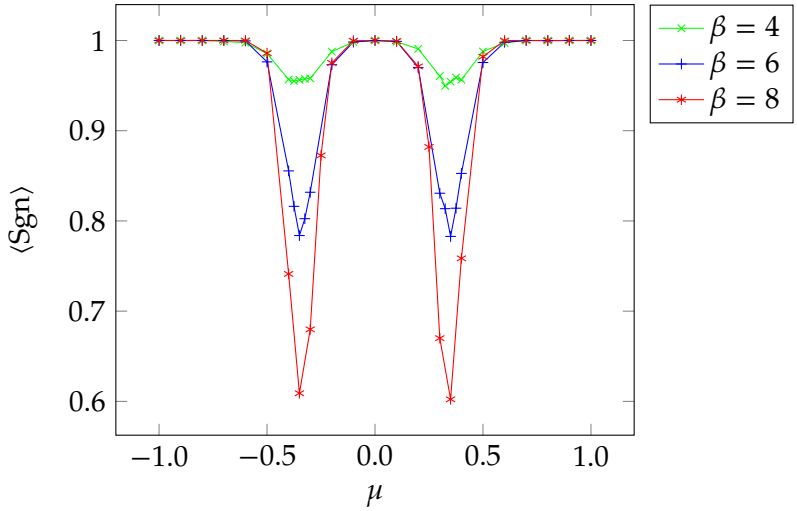

Parameters: $t = 1$, $U = 4$, $B = 0$, $\lambda_2 = 0$, $N = 4$, $n_{\text{mc}} = 2^{16}$; Lines are visual guides only

Table 6.4.: $\langle \text{Sgn} \rangle$ at $\mu = \pm 0.4 \cdot U$ for different β

	β		
μ	4	6	8
$+0.4 \cdot U$	0.9564	0.7838	0.6090
$-0.4 \cdot U$	0.9543	0.7828	0.6023

Parameters: $t = 1$, $U = 4$, $B = 0$, $\lambda_2 = 0$, $N = 4$, $n_{\text{mc}} = 2^{16}$

6.3.1. Average sign with second Ising spin

In order to study the effect a second Ising field has on $\langle \text{Sgn} \rangle$, we chose the value $\mu = 0.4 \cdot U$ at $\beta = 6$, which we deemed *bad enough* while not unnecessarily increasing the computational time. The results were plotted in Fig. 6.3.

We observe that increasing the absolute value of λ_2 seems to lead to a lower $\langle \text{Sgn} \rangle$. One would expect that the graphs are symmetric around $\lambda_2 = 0$, since $\cosh(-\lambda_2) =$

$\cosh(+\lambda_2)$. This is not the case however, and, we assume, due to bad convergence. Also, the region very close to $\lambda_2 = 0.0$ does seem to have a better $\langle \mathrm{Sgn} \rangle$, but more data needs to be generated to rule out statistical anomalies.

Figure 6.3.: $\langle \mathrm{Sgn} \rangle$ for 2 Ising spins as a function of λ_2

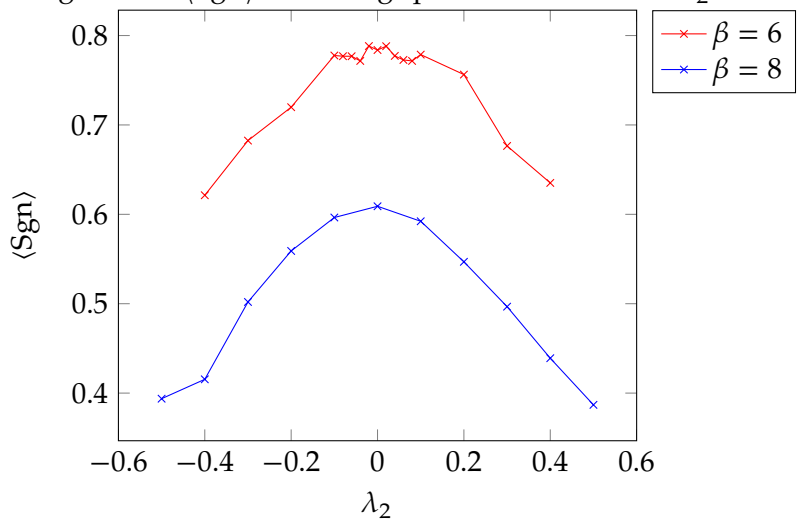

Parameters: $\beta = 6$, $t = 1$, $U = 4$, $\mu = 0.4 \cdot U$, $B = 0$, $N = 4$, $n_{\mathrm{mc}} = 2^{16}$
Lines are visual guides only

6.3.2. Distribution of Sgn and convergence

A non-trivial question is at which point in a simulation one should measure Sgn. Since we want to sample (sufficiently) statistically uncorrelated Markov configurations to get reliable measurements of the different observables, there should ideally be a sufficient number of steps in between measurements. However, when for example sampling at the end of a sweep, one might by chance get a positive sign, while all previous steps in the sweep had negative signs and vice versa. This would mean that simulation times have to be chosen even longer to get convergent data.

Figure 6.4 shows a typical distribution of signs during a simulation run. We have tracked Sgn during one sweep and averaged the signs encountered during a sweep, which we call $\langle \mathrm{Sgn} \rangle_{\mathrm{local}}$. The plot shows a representative sample of these averages for 150 consecutive sweeps. It appears that Sgn tends to stick entirely to a value of either $+1$ or -1, and only rarely are transitions to the other respective value encountered.

This distribution suggests that taking full measurements at the end of a sweep might not affect the convergence too badly. The distribution of $\langle \mathrm{Sgn} \rangle_{\mathrm{local}}$ might look different for other sets of simulation parameters, which would need to be investigated. Furthermore, it might be feasible to replace $\langle O\,\mathrm{Sgn} \rangle \to \left\langle O \langle \mathrm{Sgn} \rangle_{\mathrm{local}} \right\rangle$ in the expectation value of an observable O, cf. Eq. (3.49).

The convergence times for measurements of the sign tend to be extremely long. Fig-

Figure 6.4.: Typical distribution of Sgn averaged over over one sweep each

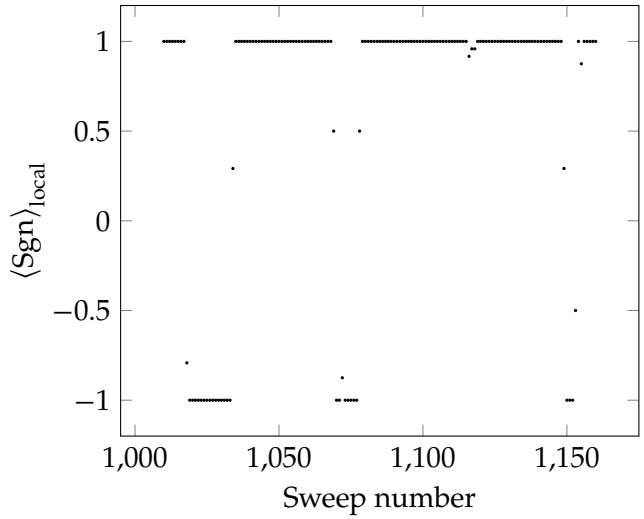

Parameters: $\beta = 6$, $t = 1$, $U = 4$, $\mu = 0.4 \cdot U$, $B = 0$, $\lambda_2 = 0.0$, $N = 4$, $n_{\mathrm{mc}} = 2^{16}$
Lines are visual guides only

ure 6.5 shows how the convergence of Sgn depends on the number n_{mc} of Monte Carlo sweeps. Here, $\langle \mathrm{Sgn} \rangle$ was calculated with respect to $\langle \mathrm{Sgn} \rangle_{\mathrm{local}}$, i.e., the signs of all configurations encountered during the sweep (up to a total of $192 \cdot 2^{16}$ measurements). We observe convergence only towards the entire number of measurements taken.

6.4. Convergence without a second Ising spin

When simulating the Hubbard model with $U > 0$ and varying B while keeping μ constant, the program starts to have convergence problems for values in the interval $B \simeq \pm[0.2, 0.6] \cdot U$. Similary, the $U < 0$ model for varying μ at constant B shows bad convergence around $\mu \simeq \pm[0.2, 0.6] \cdot U$. Below, we discuss the results of the $U > 0$ case, but the data for the $U < 0$ is qualitatively the same.

Table 6.5 shows expectation values $\langle S_z \rangle$ at $B = \pm 0.3 \cdot U$ and $\mu = 0$ for the repulsive model, where the same parameters as in Fig. 6.1 were used. The values for three representative runs are given. The mean and standard deviations are given with respect to 20 independent runs. The exact solution would be $\langle S_z \rangle = \pm 0.394$.

While except for one case the exact solution lies within error bars, the relative error is of the same order as the average. Note that the badly convergent region of B and μ correspond to the same interval where we encounter the largest sign problems.

Figure 6.5.: Convergence of Sgn for different runtimes

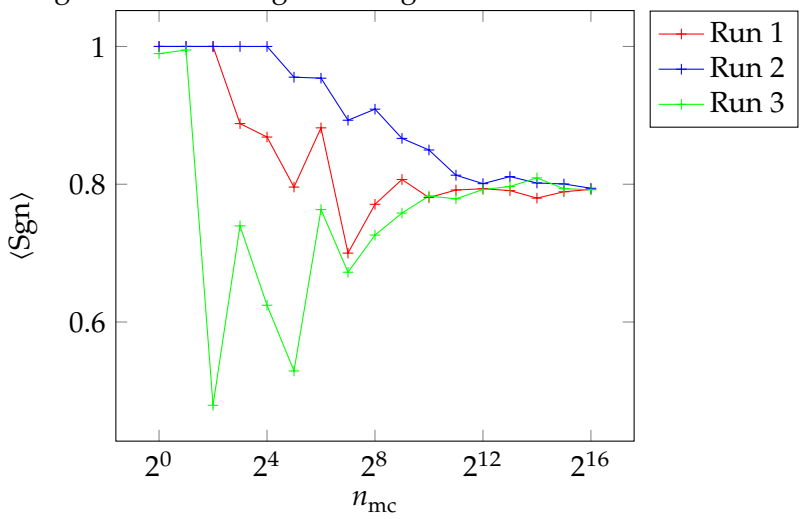

Parameters: $\beta = 6$, $t = 1$, $U = 4$, $\mu = 0.4 \cdot U$, $B = 0$, $\lambda_2 = 0.0$, $N = 4$
Lines are visual guides only

Table 6.5.: Example results of $\langle S_z \rangle$ for the repulsive model

		Run				
B	λ_2	1	2	3	avg	Δ
$+1.2$	0.0	0.4371	0.3565	0.8039	0.3209	0.2216
	0.5	0.4912	0.1168	0.0007	0.1522	0.2922
-1.2	0.0	-0.5220	-0.0002	0.5566	-0.2275	0.2587
	0.5	-0.0003	-0.4819	-0.0007	-0.0232	0.1026

Parameters: $\beta = 6$, $t = 1$, $U = 4$, $\mu = 0$, $B = 1.2 \cdot U$, $n_{\mathrm{mc}} = 2048$

7. Discussion and conclusions

Our implementation is able to recover analytic results for a system of 2 sites at well-behaved parameters. For a system of 4 particles, we can show that the average sign in the $U > 0$ Hubbard model is especially bad in the intermediate regime between half filling and complete filling ($\langle \tilde{n} \rangle = 0.0$ and $\langle n \rangle = 1.0$), and between half filling and the empty lattice ($\langle \tilde{n} \rangle = -1.0$), respectively. These regions correspond to chemical potentials around $\mu \simeq \pm 0.4 \cdot U$. Furthermore, we can show that the choice of λ_2 does affect the average sign $\langle \mathrm{Sgn} \rangle$, and that λ_2 well away from $\lambda_2 = 0$ seems to lead to worse signs.

The main difficulty in measuring Sgn is that it is a binary variable, and that the only meaningful quantity to look at is its average over a large set of measurements. In the case of physical quantities, we can expect that they will be clustered around their most likely values in a Gaussian distribution; for Sgn however there is no other way but to count how often they actually occured. While we use $|\rho|$ as a transition probability to guide the evolution of our physical system, it has nothing to do with the particular value $\mathrm{Sgn}(\rho)$ takes, which does not seem to follow a Markov process. This further implies that the standard method of giving estimates on the statistical error in Monte Carlo simulations, Eq. (3.7), is not applicable: the square term is always going to be $\left\langle \mathrm{Sgn}^2 \right\rangle = 1$, and the error estimate will scale with the number n of measured Sgn, even though $\langle \mathrm{Sgn} \rangle$ might be far away from the actual value.

Therefore the only way out is to perform a number of sufficiently long simulations with the same parameters and calculate the variance between the $\langle \mathrm{Sgn} \rangle$ obtained for each of the runs. We were not able to do that because of constraints in computer power.

Furthermore, in a system of $N = 2$ sites, where we did not encounter a sign problem, the simulation shows bad convergence for the attractive $U < 0$ Hubbard model without a magnetic field $B = 0$ and at varying chemical potential μ. We encountered the worst convergence in the interval $\mu = \pm[0.2, 0.6] \cdot U$, which coincides with the problematic region when analyzing Sgn. Since our modified discrete Hubbard-Stratonovich transformation is essentially an interpolation between the Hirsch ($U > 0$) and anti-Hirsch ($U < 0$) algorithms, we can assume that our study of these regimes is also affected by convergence problems.

The bad convergence might be related to the system getting stuck in certain spin configurations[27], which might be improved by introducing global moves into the simulation.

7.1. Outlook

In general, our setup for performing thorough numerical investigations of the sign problem was inadequate. While we were able to implement a robust prototype of the simulation and obtain preliminary results, the study has to be performed on a cluster of machines to obtain a larger number of numerical measurements to perform proper statistical analyses. More powerful computational resources are also needed to study larger systems, i.e., in two dimensions, and particularly to obtain measurements of physical parameters from the Green's functions, which are almost as computationally demanding as running the pure Monte Carlo dynamics.

Apart from improving the ergodicity by using global moves, the computational complexity of the algorithm can be reduced by implementing delayed updating of the Green's function[28], which should significantly improve the runtime of a sweep through the lattice. Also, since the potential terms enter the simulation as sparse matrices, we could use a Trotter-decomposition to break up the kinetic term into sparse matrices for every lattice dimension. This is viable, if this additional breakup does not significantly increase the statistical errors, as sparse linear algebra routines are generally faster compared to the dense ones we are employing.

In [29] it is suggested that while different Hubbard-Stratonovich transformations might lead to worse average signs, they might still be a good choice if they show better convergence properties. Furthermore, Hartree mean-field calculations[30] suggest that a complex-valued factor λ_2 as well as using domain-walls in a two-dimensional lattice might lead to better results. For this, we could for example choose $\lambda_2 \neq 0$ along a domain-wall, and $\lambda_2 = 0$ inside the domains.

In addition to generating a statistically significant amount of data, we suggest that future studies should therefore investigate how the convergence of the determinantal Quantum Monte Carlo simulation is affected by different choices of λ_2, and in particular, how convergence and average sign could be influenced by choosing λ_2 different on every lattice point.

Bibliography

[1] J. E. Hirsch. Two-dimensional Hubbard model: Numerical simulation study. *Physical Review B*, **31**: 4403, 1985.

[2] Elliott H. Lieb and F. Y. Wu. Absence of Mott Transition in an Exact Solution of the Short-Range, One-Band Model in One Dimension. *Physical Review Letters*, **21**: 192–192, 1968. doi: 10.1103/PhysRevLett.21.192.2

[3] J. E. Hirsch et al. Monte Carlo simulations of one-dimensional fermion systems. *Physical Review B*, **26**: 5033, 1982.

[4] R. Blankenbecler and R. L. Sugar. Projector Monte Carlo method. *Physical Review D*, **27**: 1304–1311, 1983. doi: 10.1103/PhysRevD.27.1304

[5] R. Blankenbecler, D. J. Scalapino, and R. L. Sugar. Monte Carlo calculations of coupled boson-fermion systems. I. *Physical Review D*, **24**: 2278, 1981.

[6] E. Y. Loh et al. Sign problem in the numerical simulation of many-electron systems. *Physical Review B*, **41**: 9301–9307, 1990. doi: 10.1103/PhysRevB.41.9301

[7] Ghassan George Batrouni and Philippe de Forcrand. Fermion sign problem: Decoupling transformation and simulation algorithm. *Physical Review B*, **48**: 589–592, 1993. doi: 10.1103/PhysRevB.48.589

[8] Matthias Troyer and Uwe-Jens Wiese. Computational Complexity and Fundamental Limitations to Fermionic Quantum Monte Carlo Simulations. *Physical Review Letters*, **94**: 170201, 2005. doi: 10.1103/PhysRevLett.94.170201

[9] Alexander Altland and Ben Simons. *Condensed matter field theory*. 2nd ed Cambridge ; New York: Cambridge University Press, 2010. 770 pp. isbn: 9780521769754

[10] Fabian H. L Essler. *The one-dimensional Hubbard model*. English; Cambridge: Cambridge University Press, 2010. isbn: 9780521143943 0521143942

[11] Matthias Troyer "Classical and quantum monte carlo algorithms and exact diagonalization" 2004

[12] Werner Krauth. *Statistical mechanics algorithms and computations*. English; Oxford: Oxford University Press, 2006. isbn: 9781429459501 1429459506

[13] Wolfgang von der Linden. A quantum Monte Carlo approach to many-body physics. *Physics Reports*, **220**: 53–162, 1992 issn: 0370-1573. doi: 10.1016/0370-1573(92)90029-Y

[14] Manfred Salmhofer. *Renormalization: an introduction*. English; Berlin: Springer Verlag, 2010. isbn: 3642084303 9783642084300

[15] J. E. Hirsch. Discrete Hubbard-Stratonovich transformation for fermion lattice models. *Physical Review B*, **28**: 4059, 1983.

[16] Ghassan George Batrouni and Richard T. Scalettar. Anomalous decouplings and the fermion sign problem. *Physical Review B*, **42**: 2282–2289, 1990. doi: 10.1103/PhysRevB.42.2282

[17] J. Hirsch. Erratum: Discrete Hubbard-Stratonovich transformation for fermion lattice models. *Physical Review B*, **29**: 4159–4159, 1984 issn: 0163-1829. doi: 10.1103/PhysRevB.29.4159

[18] Edwin Langmann "Monte Carlo algorithms for the 2D Hubbard model" Private communications 2011

[19] Jr E. Y. Loh et al. In: *Stable Matrix-Multiplication Algorithms for Low-Temperature Numerical Simulations of Fermions*. Dionys Baeriswyl and David K. Campbell, eds. 55–60. Springer US, 1990. isbn: 978-1-4612-7869-6, 978-1-4613-0565-1

[20] .*SciPy.org — SciPy.org*, url: http://www.scipy.org/ (visited on 07/07/2013)

[21] .*What is HDF5?*, url: http://www.hdfgroup.org/HDF5/whatishdf5.html (visited on 07/08/2013)

[22] .*Intel® Math Kernel Library – Documentation | Intel® Developer Zone*, url: http://software.intel.com/en-us/articles/intel-math-kernel-library-documentation (visited on 07/07/2013)

[23] .*QUEST*, url: http://quest.ucdavis.edu/index.html (visited on 07/07/2013)

[24] C. N. Varney et al. Quantum Monte Carlo study of the two-dimensional fermion Hubbard model. *Physical Review B*, **80**: 075116, 2009. doi: 10.1103/PhysRevB.80.075116

[25] S. R. White et al. Numerical study of the two-dimensional Hubbard model. *Physical Review B*, **40**: 506, 1989.

[26] Karl-Oskar Backlund. *Deriving an extended one-band Hubbard model for cuprate superconductors*. 2011.

[27] Richard T. Scalettar, Reinhard M. Noack, and Rajiv R. P. Singh. Ergodicity at large couplings with the determinant Monte Carlo algorithm. *Physical Review B*, **44**: 10502–10507, 1991. doi: 10.1103/PhysRevB.44.10502

[28] Phani K. V. V. Nukala et al. Fast update algorithm for the quantum Monte Carlo simulation of the Hubbard model. *Physical Review B*, **80**: 195111, 2009. doi: 10.1103/PhysRevB.80.195111

[29] Liang Chen and A.-M.S. Tremblay. Determinant Monte Carlo for the Hubbard Model with Arbitrarily Gauged Auxiliary Fields. *International Journal of Modern Physics B*, **06**: 547–560, 1992 issn: 0217-9792, 1793-6578. doi: 10.1142/S0217979292000323

[30] Edwin Langmann and Mats Wallin. Mean Field Magnetic Phase Diagrams for the Two Dimensional t — t — U Hubbard Model. *Journal of Statistical Physics*, **127**: 825–840, 2007 issn: 0022-4715, 1572-9613. doi: 10.1007/s10955-007-9308-y

A. Explicitly taking the fermion trace

We want to show that Fock traces over bilinear Fermion operators can be taken explicitly and give a one-particle determinant. A completely orthonormal basis for a Fock Space of N particles is formed by

$$\left|\left\{n_\mu\right\}\right\rangle = \left(c_1^\dagger\right)^{n_1}\left(c_2^\dagger\right)^{n_2}\cdots\left(c_N^\dagger\right)^{n_N}|0\rangle, \tag{A.1}$$

where the state j can be occupied by at most one particle, $n_j \in \{0,1\}$, which gives a 2^N states. $|0\rangle$ is defined as the state that does not contain particles. $c_i^\dagger$ and c_i are Fermionic creation and annihilation operators in second quantized form acting on a state in Fock space and are defined by:

$$\{c_i, c_j^\dagger\} = \delta_{ij} \tag{A.2a}$$

$$\{c_i, c_j\} = 0 \tag{A.2b}$$

$$c_j|0\rangle = 0. \tag{A.2c}$$

Bilinear Fermion operators are of the form

$$\hat{A} = \sum_{i,j} \mathbf{A}_{ij} c_i^\dagger c_j, \tag{A.3}$$

should be read as $k \cong (\sigma, l)$ with l the position-index in one dimension (or $k \cong (\sigma, l_x, l_y)$ in two dimensions).

The lemma to be proven is then:

Lemma 1 *The Fock-space trace* Tr_F *over a product of exponentials of operators of the form Eq.* (A.3) *is given by the one-particle determinant:*

$$\operatorname*{Tr}_F\left(\mathrm{e}^{\hat{A}_1}\mathrm{e}^{\hat{A}_2}\cdots\mathrm{e}^{\hat{A}_k}\right) = det_{N\times N}\left(\mathbb{1} + \mathrm{e}^{\mathbf{A}_1}\mathrm{e}^{\mathbf{A}_2}\cdots\mathrm{e}^{\mathbf{A}_k}\right). \tag{A.4}$$

□

In oder to prove this, we also need to show the following two lemmata:

Lemma 2 *For the commutator of two operators* $\hat{A}$ *and* $\hat{B}$ *of the form Eq.* (A.3),

$$\left[\hat{A}, \hat{B}\right] = \hat{C}, \tag{A.5}$$

the resulting operator $\hat{C}$ *is also of the form Eq.* (A.3) *with:*

$$\mathbf{C} = [\mathbf{A}, \mathbf{B}]. \tag{A.6}$$

□

Lemma 3 *A product of exponentials of k operators $\hat{A}_k$ gives an exponential of a bilinear operator of the form Eq.* (A.3)*:*

$$\mathrm{e}^{\hat{A}_1}\mathrm{e}^{\hat{A}_2}\cdots\mathrm{e}^{\hat{A}_k} = \mathrm{e}^{\hat{D}}, \tag{A.7}$$

with the matrix elements of $\hat{D}$ given by

$$\mathrm{e}^{\mathbf{A}_1}\mathrm{e}^{\mathbf{A}_2}\cdots\mathrm{e}^{\mathbf{A}_k} = \mathrm{e}^{\mathbf{D}} \tag{A.8}$$

□

Proof (of Lemma 2) We start by writing the left-hand side of Eq. (A.5) explicitly :

$$\left[\hat{A},\hat{B}\right] = \sum_{ijkl}\mathbf{A}_{ij}\mathbf{B}_{kl}c_i^\dagger c_j c_k^\dagger c_l - \sum_{ijkl}\mathbf{B}_{ij}\mathbf{A}_{kl}c_i^\dagger c_j c_k^\dagger c_l, \tag{A.9a}$$

but the matrix elements are just numbers and we can shift indices at will:

$$= \sum_{ijkl}\mathbf{A}_{ij}\mathbf{B}_{kl}\left(c_i^\dagger c_j c_k^\dagger c_l - c_k^\dagger c_l c_i^\dagger c_j\right) \tag{A.9b}$$

$$= \sum_{ijkl}\mathbf{A}_{ij}\mathbf{B}_{kl}\left[c_i^\dagger c_j, c_k^\dagger c_l\right], \tag{A.9c}$$

which we can express in terms of the anti-commutator:

$$= \sum_{ijkl}\mathbf{A}_{ij}\mathbf{B}_{kl}\left(c_i^\dagger\left\{c_j, c_k^\dagger\right\}c_l - c_k^\dagger\{c_l, c_i^\dagger\}c_j\right). \tag{A.9d}$$

Using the canonical anti-commutation relation Eq. (A.2a), summing over both delta-functions and renaming $k \to i, j \leftrightarrow l$ in the second term yields the required form:

$$= \sum_{ijl} c_i^\dagger c_l\left(\mathbf{A}_{i,j}\mathbf{B}_{j,l} - \mathbf{B}_{i,j}\mathbf{A}_{j,l}\right). \tag{A.9e}$$

■

Proof (of Lemma 3) The case $k = 1$ is trivial. For the case $k = 2$ we get, using the Baker-Campbell-Hausdorff formula (without writing higher-order commutators explicitly):

$$\mathrm{e}^{\hat{A}_1}\mathrm{e}^{\hat{A}_2} = \mathrm{e}^{\hat{D}} = \mathrm{e}^{\hat{A}_1+\hat{A}_2+\frac{1}{2}\left[\hat{A}_1,\hat{A}_2\right]+\frac{1}{12}\left[\hat{A}_1,\left[\hat{A}_1,\hat{A}_2\right]\right]-\frac{1}{12}\left[\hat{A}_2,\left[\hat{A}_1,\hat{A}_2\right]\right]+\cdots}, \tag{A.10}$$

and so the operator $\hat{D}$ is given by a linear combination of $\hat{A}_1$, $\hat{A}_2$, $\left[\hat{A}_1,\hat{A}_2\right]$ and commutator nestings thereof. We need to show the matrix $\mathbf{D}$ in $\hat{D}$ is given by (dropping the constants for convenience):

$$\mathbf{D} = \mathbf{A}_1 + \mathbf{A}_2 + [\mathbf{A}_1,\mathbf{A}_2] + [\mathbf{A}_1,[\mathbf{A}_1,\mathbf{A}_2]] - [\mathbf{A}_2,[\mathbf{A}_1,\mathbf{A}_2]] + \cdots, \tag{A.11}$$

Specifically we need to show that a combination of nested commutators of operators of the form Eq. (A.3) is again an operator $\hat{B}$ of the same form:

$$\hat{B} = \left[\hat{A}_{i_l},\left[\hat{A}_{i_{l-1}},\left[\cdots,\left[\hat{A}_{i_2},\hat{A}_{i_1}\right]\right]\right]\right], \tag{A.12a}$$

with its matrix elements given by:

$$\mathbf{B} = \left[\mathbf{A}_{i_l}, \left[\mathbf{A}_{i_{l-1}}, \left[\cdots, \left[\mathbf{A}_{i_2}, \mathbf{A}_{i_1}\right]\right]\right]\right], \tag{A.12b}$$

where $i_l \in \{1, 2\}$ represent the permissible combinations of $\hat{A}_1$ and $\hat{A}_2$. Assume that Eq. (A.12) holds for a product of l matrices. Then the case $l + 1$ reads:

$$\left[\hat{A}_{i_{l+1}}, \left[\hat{A}_{i_l}, \left[\hat{A}_{i_{l-1}}, \left[\cdots, \left[\hat{A}_{i_2}, \hat{A}_{i_1}\right]\right]\right]\right]\right] = \left[\hat{A}_{i_{l+1}}, \hat{B}\right] = \hat{B}', \tag{A.13}$$

and by Lemma 2:

$$\left[\mathbf{A}_{i_{l+1}}, \left[\mathbf{A}_{i_l}, \left[\mathbf{A}_{i_{l-1}}, \left[\cdots, \left[\mathbf{A}_{i_2}, \mathbf{A}_{i_1}\right]\right]\right]\right]\right] = \mathbf{B}'. \tag{A.14}$$

Since $\hat{D}$ is a linear combination of operators Eq. (A.12), it automatically follows that its matrix elements are given by Eq. (A.11). The extension to a product of k exponentiated operators follows from induction. ∎

Using Lemmata 2 and 3 the proof then proceeds as follows:

Proof (of Lemma 1) The trace should be independent of the choice of basis, and so we start by changing to a basis where the operator $\hat{D}$ is digonal by performing a Bogoliubov transformation:

$$\tilde{c}_\mu = \sum_i U_{\mu i} c_i \tag{A.15a}$$

$$\tilde{c}_\mu^\dagger = \sum_i \left(U^\dagger\right)_{i\mu} c_i^\dagger, \tag{A.15b}$$

so that in that basis $\hat{D}$ takes the form:

$$\hat{D} = \sum_\mu d_\mu c_\mu^\dagger c_\mu. \tag{A.16}$$

The Hilbert space of N particles is spanned by the states generated with the $\tilde{c}_\mu^\dagger$ by acting on the vacuum state $|0\rangle$:

$$\left|\{\tilde{n}_\mu\}\right\rangle = \left(\tilde{c}_1^\dagger\right)^{\tilde{n}_1} \left(\tilde{c}_2^\dagger\right)^{\tilde{n}_2} \cdots \left(\tilde{c}_N^\dagger\right)^{\tilde{n}_N} |0\rangle, \tag{A.17}$$

where the $\tilde{n}_\mu \in \{0, 1\}$ are the eigenvalues of the operator $\tilde{c}_\mu^\dagger \tilde{c}_\mu$, i.e., the number of particles in state μ. The $\left|\{\tilde{n}_\mu\}\right\rangle$ give a complete orthonormal basis of 2^N states. Acting on the $\left|\{\tilde{n}_\mu\}\right\rangle$ with the exponent of $\hat{D}$:

$$\mathrm{e}^{\sum_\mu d_\mu c_\mu^\dagger c_\mu} \left|\{\tilde{n}_\mu\}\right\rangle = \prod_\mu \left[1 + \left(\mathrm{e}^{d_\mu} - 1\right) c_\mu^\dagger c_\mu\right] \left|\{\tilde{n}_\mu\}\right\rangle, \tag{A.18a}$$

the $\tilde{c}_\mu^\dagger \tilde{c}_\mu$ will either yield 0 or 1:

$$= \prod_\mu \mathrm{e}^{d_\mu \tilde{n}_\mu} \left|\{\tilde{n}_\mu\}\right\rangle. \tag{A.18b}$$

The trace over the fermion degrees of freedom then reads:

$$\operatorname*{Tr}_F\left(\mathrm{e}^{\hat{D}}\right) = \sum_{\{\tilde{n}_\mu\}} \left\langle \{\tilde{n}_\mu\} \left| \prod_\mu \mathrm{e}^{d_\mu \tilde{c}_\mu^\dagger \tilde{c}_\mu} \right| \{\tilde{n}_\mu\} \right\rangle \tag{A.19}$$

$$= \sum_{\{\tilde{n}_\mu\}} \left\langle \{\tilde{n}_\mu\} \left| \prod_\mu \left(1 + \left(\mathrm{e}^{d_\mu} - 1\right) \tilde{c}_\mu^\dagger \tilde{c}_\mu\right) \right| \{\tilde{n}_\mu\} \right\rangle \tag{A.20}$$

$$= \sum_{\{\tilde{n}_\mu\}} \prod_\mu \left(1 + \left(\mathrm{e}^{d_\mu} - 1\right) \tilde{n}_\mu\right) \left\langle \{\tilde{n}_\mu\} \,\middle|\, \{\tilde{n}_\mu\} \right\rangle, \tag{A.21}$$

where we use the result of Eq. (A.18) and the fact that the basis is orthonormal, we finally obtain:

$$= \prod_\mu \sum_{\tilde{n}_\mu = 0,1} \left(\mathrm{e}^{d_\mu \tilde{n}_\mu}\right), \tag{A.22}$$

$$= \det_{N \times N} \left(\mathbb{1} + \mathrm{e}^{\mathbf{D}}\right). \tag{A.23}$$

■

B. Equal-time Green's functions

We consider the single-particle Green's function in the diagonal representation (cf. Eq. (A.19)):

$$\left\langle c_i c_j^\dagger \right\rangle_s = \frac{\operatorname{Tr} c_i c_j^\dagger \prod_\nu \mathrm{e}^{d_\nu \tilde{c}_\nu^\dagger \tilde{c}_\nu}}{\prod_\nu (1 + \mathrm{e}^{d_\nu})} \tag{B.1a}$$

$$= \sum_{\nu'} \langle\, \nu' \,|\, i \rangle \langle\, j \,|\, \nu' \rangle \frac{\operatorname{Tr} c_{\nu'} c_{\nu'}^\dagger \prod_\nu \mathrm{e}^{d_\nu \tilde{c}_\nu^\dagger \tilde{c}_\nu}}{\prod_\nu (1 + \mathrm{e}^{d_\nu})}. \tag{B.1b}$$

Writing the trace explicitly, we get:

$$\operatorname{Tr} \tilde{c}_{\nu'} \tilde{c}_{\nu'}^\dagger \prod_\nu \mathrm{e}^{d_\nu \tilde{c}_\nu^\dagger \tilde{c}_\nu} = \sum_{\{\tilde{n}_\mu\}} \langle\, \{\tilde{n}_\mu\} \,|\, \tilde{c}_{\nu'} \tilde{c}_{\nu'}^\dagger \prod_\nu \mathrm{e}^{d_\nu \tilde{c}_\nu^\dagger \tilde{c}_\nu} |\, \{\tilde{n}_\mu\} \rangle \tag{B.2a}$$

$$= \sum_{\{\tilde{n}_\mu\}} (1 - \tilde{n}_{\nu'}) \mathrm{e}^{d_{\nu'} \tilde{n}_{\nu'}} \prod_{\nu \neq \nu'} \mathrm{e}^{d_\nu \tilde{n}_\nu}, \tag{B.2b}$$

and we see directly that only states with $n_{\nu'} = 0$ contribute to the sum:

$$= \prod_{\nu \neq \nu'} \sum_{\tilde{n}_\nu = 0,1} \mathrm{e}^{d_\nu \tilde{n}_\nu} \tag{B.2c}$$

The Green's function then becomes:

$$\left\langle c_i c_j^\dagger \right\rangle_s = \frac{\sum_{\nu'} \langle\, \nu' \,|\, i \rangle \langle\, j \,|\, \nu' \rangle}{1 + \mathrm{e}^{d_{\nu'}}} \tag{B.3}$$

$$= \left[\frac{\mathbb{1}}{\left(\mathbb{1} + \prod_l^L B_l \right)} \right]_{ij} \equiv (g)_{ij}. \tag{B.4}$$

The result can be generalized to any equal-time Green's function at the l-th timeslice:

$$g^\sigma(l) \equiv \left(\mathbb{1} + B_{l+1} \cdots B_{L-1} B_L B_1 \cdots B_l \right)^{-1}, \tag{B.5}$$

where we have reinserted the spin-index σ.

C. Simplification of transition probabilities

The ratios in the transition probabilities Eq. (4.1) can be written in terms of the Green's functions, Eq. (3.43). The crucial identity is the commutativity property of two matrices of equal size, $\mathbf{A}$ and $\mathbf{B}$, under the determinant:

$$\det(\mathbf{AB}) = \det(\mathbf{BA}) \tag{C.1}$$

We then write:

$$R^\sigma = \frac{\det\left(\mathbb{1} + \mathbf{B}_1^\sigma \cdots \mathbf{B}_l^\sigma \triangle^\sigma(l) \cdots \mathbf{B}_L^\sigma\right)}{\det\left(\mathbb{1} + \mathbf{B}_1^\sigma \cdots \mathbf{B}_l^\sigma \cdots \mathbf{B}_L^\sigma\right)} \tag{C.2}$$

$$= \det\left(\frac{\mathbb{1} + \mathbf{B}_1^\sigma \cdots \mathbf{B}_l^\sigma \triangle^\sigma(l) \cdots \mathbf{B}_L^\sigma}{\mathbb{1} + \mathbf{B}_1^\sigma \cdots \mathbf{B}_l^\sigma \cdots \mathbf{B}_L^\sigma}\right), \tag{C.3}$$

where identities $\mathbb{1} = \mathbf{B}_m^{-1}\mathbf{B}_m$ up to $\mathbf{B}_l$ are inserted in the and Eq. (C.1) is used repeatedly to obtain:

$$= \frac{\det\left(\mathbb{1} + \mathbf{B}_{l+1}^\sigma \mathbf{B}_{l+2}^\sigma \cdots \mathbf{B}_L^\sigma \mathbf{B}_1^\sigma \cdots \mathbf{B}_l^\sigma \triangle^\sigma(l)\right)}{\det\left(\mathbb{1} + \mathbf{B}_{l+1}^\sigma \mathbf{B}_{l+2}^\sigma \cdots \mathbf{B}_L^\sigma \mathbf{B}_1^\sigma \cdots \mathbf{B}_L^\sigma\right)} \tag{C.4}$$

$$= \frac{\det\left(\mathbb{1} + \mathbf{M}^\sigma(l)\triangle^\sigma(l)\right)}{\det(\mathbb{1} + \mathbf{M}^\sigma(l))} \tag{C.5}$$

which can now be written in terms of the Green's function Eq. (3.43):

$$= \det\left[\mathbb{1} + (\mathbb{1} - g^\sigma(l))\left(\triangle^\sigma(l) - \mathbb{1}\right)\right], \tag{C.6}$$

where by Eq. (4.4) the matrix $\triangle^\sigma(l) - \mathbb{1}$ gives a non-zero contribution only for the i-th element on the diagonal:

$$R^\sigma = 1 + \left[1 - \left(g^\sigma(l)\right)_{ii}\right] \cdot \left[\mathrm{e}^{2\sigma\lambda s_i(l)} - 1\right]. \tag{C.7}$$

D. Cases without sign problems

The attractive Hubbard model with $U < 0$ does not suffer from a sign problem under the transformation Eq. (3.32). Applying the transformation and writing out the resulting partition function, one obtains:

$$Z = \left(\tfrac{1}{2}\mathrm{e}^{-\frac{1}{4}|U|\Delta\tau}\mathrm{e}^{\Delta\tau\mu}\right)^{L\cdot N} \operatorname*{Tr}_s \operatorname{Tr} \prod_{l=1}^{L} \prod_{\sigma=\uparrow,\downarrow} \mathrm{e}^{-\Delta\tau H_{0,\sigma}} \mathrm{e}^{\sum_i \left(s_{i,l}\lambda(n_{\sigma,i}-\frac{1}{2})+\Delta\tau(\mu+\sigma B)n_{\sigma,i}\right)} \tag{D.1}$$

$$= \left(\tfrac{1}{2}\mathrm{e}^{-\frac{1}{4}|U|\Delta\tau}\mathrm{e}^{\Delta\tau\mu}\right)^{L\cdot N} \operatorname*{Tr}_s \mathrm{e}^{-\sum_{i,l} s_{i,l}\lambda} \operatorname{Tr} \prod_{l=1}^{L} \prod_{\sigma=\uparrow,\downarrow} \mathrm{e}^{-\Delta\tau H_{0,\sigma}} \mathrm{e}^{\sum_i \left(s_{i,l}\lambda+\Delta\tau(\mu+\sigma B)\right)n_{\sigma,i}}. \tag{D.2}$$

Compared to Eq. (3.35b), in the potential matrix the sign of the spin, σ, no longer couples to the auxiliary fields,

$$\left(V^{\sigma}(l)\right)_{ij} = \delta_{ij}\left[\lambda s_i(l) + \Delta\tau(\mu + \sigma B)\right]. \tag{D.3}$$

With $B = 0$, which otherwise breaks the symmetry between up- and down-spins, and after tracing out the fermion degrees of freedom, we get

$$\det O^{\uparrow} = \det O^{\downarrow} \tag{D.4}$$

in the expression for the partition function. The product of fermion determinants, which we take as the transition probability, is therefore always positive definite.

Similarly for the half-filled case at $\mu = 0$ and without a magnetic field, one can show that there is no sign problem: Using the transformation Eq. (2.22d), the repulsive model maps onto the attractive one, $U \to -U$. In particular, we take the spin-down part of Eq. (3.40), which is already transformed by the discrete Hubbard-Stratonovich transformation, and write:

$$\det O^{\downarrow} = \operatorname{Tr} \prod_{l=1}^{L} \mathrm{e}^{-\Delta\tau H_{0,\downarrow}} \mathrm{e}^{\sum_i s_i(l)\lambda n_{\downarrow,i}}, \tag{D.5a}$$

which becomes (cf. Eq. (2.16):

$$= \operatorname{Tr} \prod_{l=1}^{L} \mathrm{e}^{-\Delta\tau H_{0,\downarrow}} \mathrm{e}^{\sum_i s_i(l)\lambda\left(1-n_{\downarrow,i}\right)}, \tag{D.5b}$$

which is just the same as the spin-up determinant times the Ising-term:

$$= \mathrm{e}^{\sum_{i,l} s_i(l)\lambda} \det O^{\uparrow}, \tag{D.5c}$$

and thus the transition probability is also always positive definite.